LIBRARY OF CASE STUDIES

Contents

Case Study 1 Materials Selection for a Torsionally Stressed Cylindrical Shaft

Learning Objectives

After studying this case study, you should be able to do the following:

1. Briefly describe how the strength performance index for a solid cylindrical shaft is determined.
2. Explain the manner in which materials selection charts are employed in the materials selection process.

CS1.1 INTRODUCTION

Selection of the appropriate material is an important consideration in engineering design; that is, for some application, choosing a material having a desirable or optimum property or combination of properties. Selection of the proper material can reduce costs and improve performance. Elements of this materials selection process involve deciding on the constraints of the problem and, from these, establishing criteria that can be used in materials selection to maximize performance.

The component or structural element we have chosen to discuss is a solid cylindrical shaft that is subjected to a torsional stress. Strength of the shaft will be considered in detail, and criteria will be developed for maximizing strength with respect to both minimum material mass and minimum cost. Other parameters and properties that may be important in this selection process are also discussed briefly.

CS1.2 STRENGTH CONSIDERATIONS

For this portion of the design problem, we will establish a criterion for selection of lightweight and strong materials for the shaft. We will assume that the twisting moment and length of the shaft are specified, whereas the radius (or cross-sectional area) may be varied. We develop an expression for the mass of material required in terms of twisting moment, shaft length, and density and strength of the material. Using this expression, it will be possible to evaluate the performance—that is, maximize the strength of the torsionally stressed shaft with respect to mass and, in addition, relative to material cost.

Consider the cylindrical shaft of length L and radius r, as shown in Figure CS1.1. The application of twisting moment (or torque) M_t produces an angle of twist ϕ. Shear stress τ at radius r is defined by the equation

$$\tau = \frac{M_t r}{J} \tag{CS1.1}$$

Here, J is the polar moment of inertia, which for a solid cylinder is

$$J = \frac{\pi r^4}{2} \tag{CS1.2}$$

Thus,

$$\tau = \frac{2M_t}{\pi r^3} \tag{CS1.3}$$

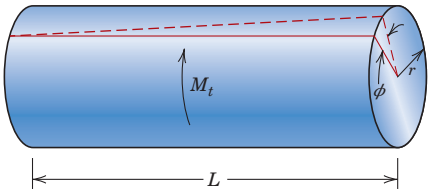

Figure CS1.1 A solid cylindrical shaft that experiences an angle of twist ϕ in response to the application of a twisting moment M_t.

A safe design calls for the shaft to be able to sustain some twisting moment without fracture. In order to establish a materials selection criterion for a light-weight and strong material, we replace the shear stress in Equation CS1.3 with the shear strength of the material τ_f divided by a factor of safety N, as

$$\frac{\tau_f}{N} = \frac{2M_t}{\pi r^3} \tag{CS1.4}$$

It is now necessary to take into consideration material mass. The mass m of any given quantity of material is just the product of its density (ρ) and volume. Since the volume of a cylinder is just $\pi r^2 L$, then

$$m = \pi r^2 L \rho \tag{CS1.5}$$

or, the radius of the shaft in terms of its mass is

$$r = \sqrt{\frac{m}{\pi L \rho}} \tag{CS1.6}$$

Substituting this r expression into Equation CS1.4 leads to

$$\frac{\tau_f}{N} = \frac{2M_t}{\pi\left(\sqrt{\frac{m}{\pi L \rho}}\right)^3} = 2M_t\sqrt{\frac{\pi L^3 \rho^3}{m^3}} \tag{CS1.7}$$

Solving this expression for the mass m yields

For a cylindrical shaft of length L and radius r that is stressed in torsion, expression for mass in terms of density and shear strength of the shaft material

$$m = (2NM_t)^{2/3}(\pi^{1/3}L)\left(\frac{\rho}{\tau_f^{2/3}}\right) \tag{CS1.8}$$

The parameters on the right-hand side of this equation are grouped into three sets of parentheses. Those contained within the first set (i.e., N and M_t) relate to the safe functioning of the shaft. Within the second set of parentheses is L, a geometric parameter. Finally, the material properties of density and strength are contained within the last set.

The upshot of Equation CS1.8 is that the best materials to be used for a light-weight shaft that can safely sustain a specified twisting moment are those having low $\rho/\tau_f^{2/3}$ ratios. In terms of material suitability, it is sometimes preferable to work with what is termed a *performance index, P,* which is just the reciprocal of this ratio; that is,

Strength performance index expression for a torsionally stressed cylindrical shaft

$$P = \frac{\tau_f^{2/3}}{\rho} \tag{CS1.9}$$

In this context, we want to use a material having a large performance index.

At this point, it becomes necessary to examine the performance indices of a variety of potential materials. This procedure is expedited by the use of *materials selection charts*.[1] These are plots of the values of one material property versus those of another property. Both axes are scaled logarithmically and usually span about five orders of magnitude, so as to include the properties of virtually all materials. For example, for our problem, the chart of interest is logarithm of strength versus logarithm of density, which is shown in Figure CS1.2.[2] It may be noted on this plot that materials of a particular type (e.g., woods, engineering polymers) cluster together and are enclosed within an envelope delineated with a bold line. Subclasses within these clusters are enclosed using finer lines.

Now, taking the logarithm of both sides of Equation CS1.9 and rearranging yields

$$\log \tau_f = \frac{3}{2}\log \rho + \frac{3}{2}\log P \tag{CS1.10}$$

This expression tells us that a plot of $\log \tau_f$ versus $\log \rho$ will yield a family of straight and parallel lines all having a slope of $\frac{3}{2}$; each line in the family corresponds to a different performance index, P. These lines are termed *design guidelines,* and four have been included in Figure CS1.2 for P values of 3, 10, 30, and 100 $(\text{MPa})^{2/3}\,\text{m}^3/\text{Mg}$.[3] All materials that lie on one of these lines will perform equally well in terms of strength-per-mass basis; materials whose positions lie above a particular line will have higher performance indices, whereas those lying below will exhibit poorer performances. For example, a material on the $P = 30$ line will yield the same strength with one-third the mass as another material that lies along the $P = 10$ line.

The selection process now involves choosing one such line, a "guideline" that has been displaced upward (while maintaining the same slope) so as to include a relatively small subset of these materials; for example, we have chosen to use the guideline corresponding to $P = 15\ (\text{MPa})^{2/3}\text{m}^3/\text{Mg}$, as represented in Figure CS1.3. Materials lying along this line or above it are in the "search region" of the diagram and are possible candidates for this rotating shaft. These include wood products, some plastics, a number of engineering alloys, the engineering composites, glasses, and engineering ceramics. On the basis of fracture toughness considerations, the engineering ceramics and glasses are ruled out as possibilities.

Furthermore, we would also like for the cylindrical shaft to exhibit some level of strength, let's say a minimum of 100 MPa. This constraint may be represented on the materials selection chart by a horizontal line constructed at 100 MPa, Figure CS1.3. Now the search region is further restricted to the area above both of these lines. Thus, most wood products and virtually all engineering polymers, as well as some engineering alloys, are eliminated as candidates; high-strength steels, high-strength aluminum and magnesium alloys, most titanium alloys, and the engineering composites remain as possibilities.

At this point, we are in a position to evaluate and compare the strength performance behavior of specific materials. Table CS1.1 presents the density, strength, and strength performance index for three engineering alloys and two engineering composites, which were deemed acceptable candidates from the analysis using the materials selection chart. In this table, strength was taken as 0.6 times the tensile yield strength (for the alloys) and 0.6 times the tensile strength (for the composites); these approximations were necessary

---

[1]A comprehensive collection of these charts may be found in M. F. Ashby, *Materials Selection in Mechanical Design,* 4th edition, Butterworth-Heinemann, Woburn, UK, 2011.

[2]Strength for metals and polymers is taken as yield strength; for ceramics and glasses, compressive strength; for elastomers, tear strength; and for composites, tensile failure strength.

[3]Please note that the abbreviation "Mg" represents the unit of megagram (10^6 grams)—not the element magnesium. Furthermore, it is the case that $1\ \text{Mg/m}^3 = 1\ \text{g/cm}^3$.

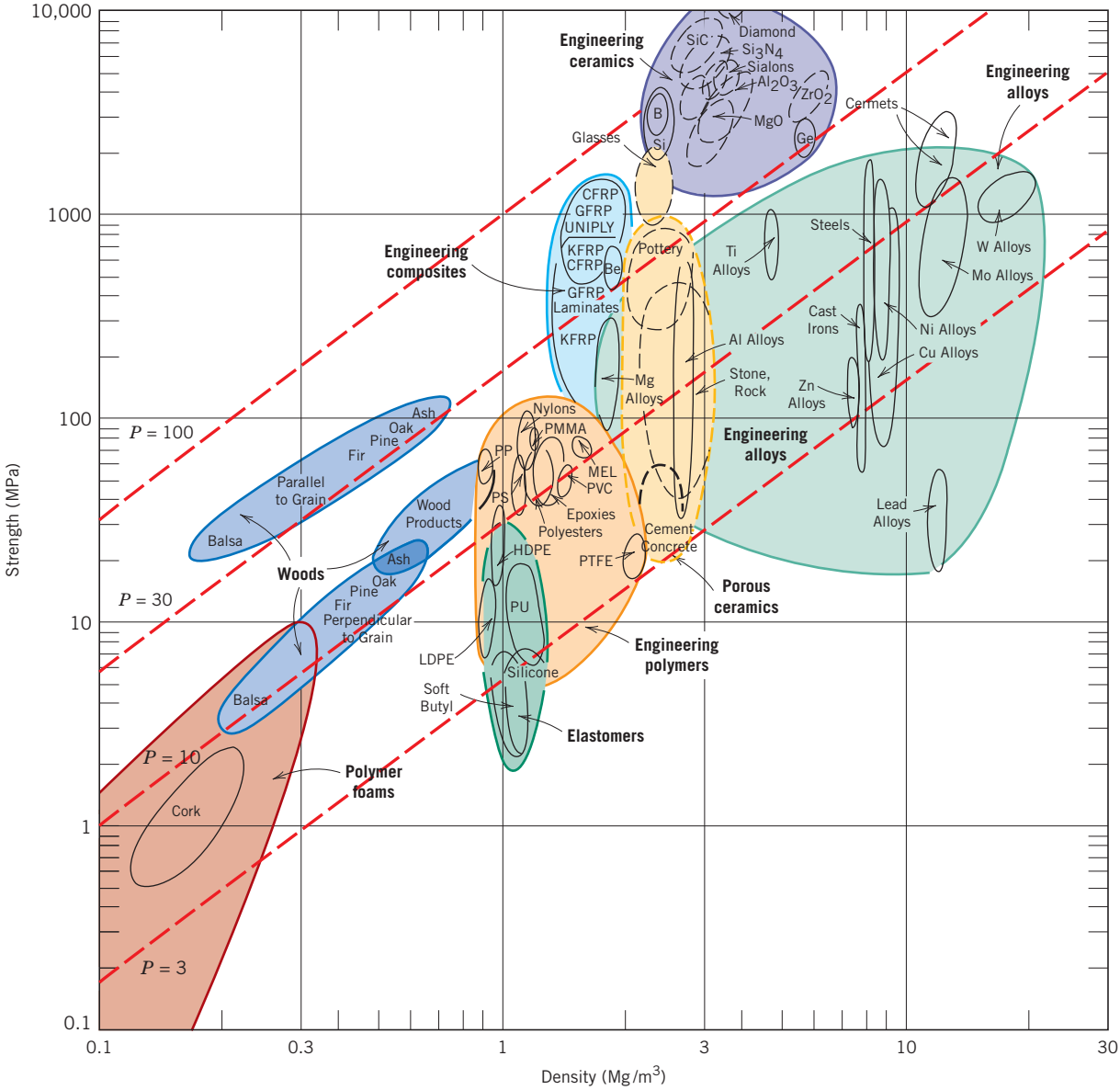

Figure CS1.2 Strength versus density materials selection chart. Design guidelines for performance indices of 3, 10, 30, and 100 $(MPa)^{2/3}m^3/Mg$ have been constructed, all having a slope of $\frac{3}{2}$.
(Adapted from M. F. Ashby, *Materials Selection in Mechanical Design*. Copyright © 1992. Reprinted by permission of Butterworth-Heinemann Ltd.)

because we are concerned with strength in torsion, and torsional strengths are not readily available. Furthermore, for the two engineering composites, it is assumed that the continuous and aligned glass and carbon fibers are wound in a helical fashion and at a 45° angle referenced to the shaft axis[4]. The five materials in Table CS1.1 are ranked according to strength performance index, from highest to lowest: carbon fiber–reinforced and glass fiber–reinforced composites, followed by aluminum, titanium, and 4340 steel alloys.

[4]You may want to view the figure in the Processing of Fiber-Reinforced Composites section (Filament Winding subsection) found in the Composites chapter of the print textbook.

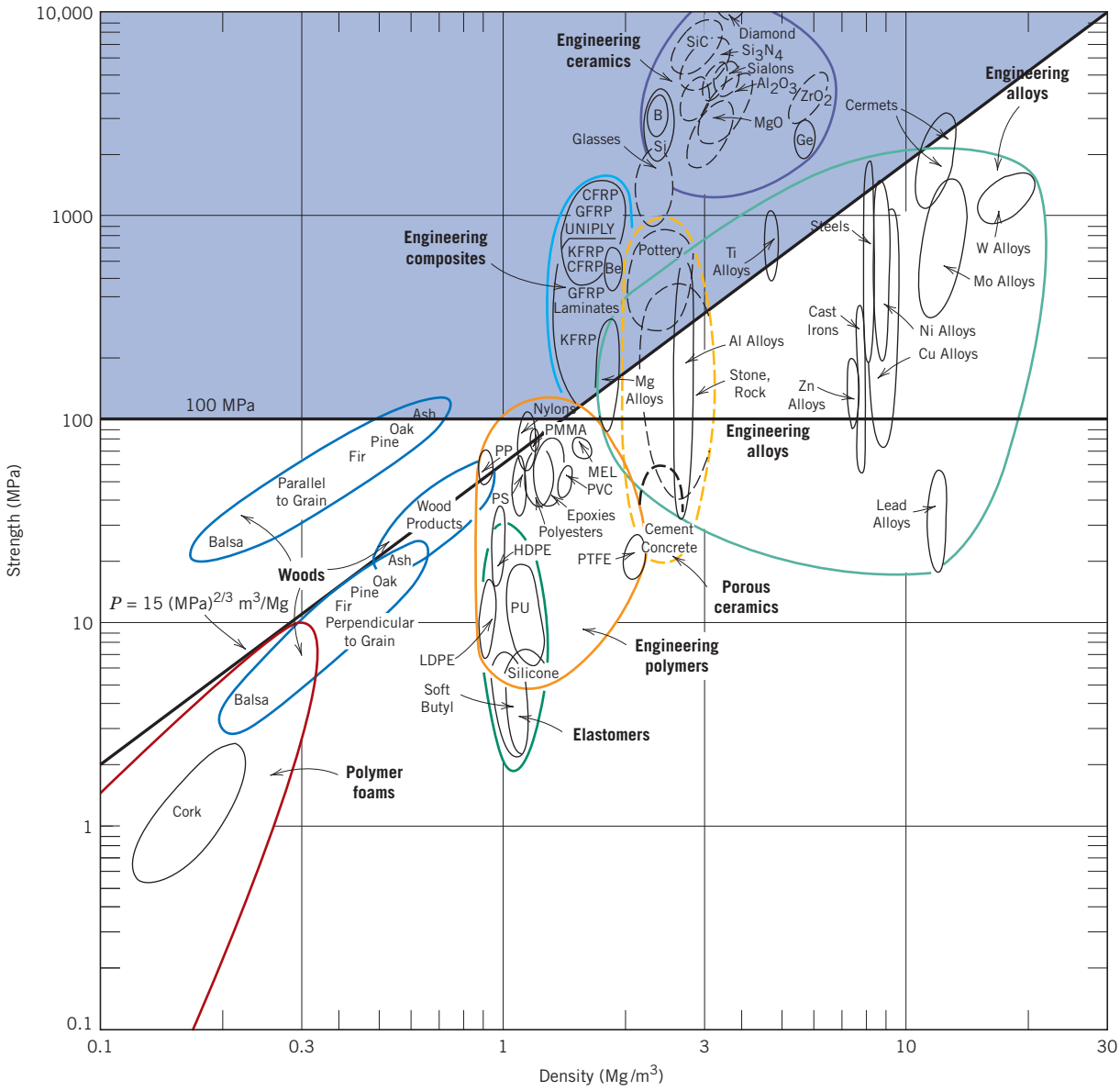

Figure CS1.3 Strength versus density materials selection chart. Materials within the shaded region are acceptable candidates for a solid cylindrical shaft that has a mass-strength performance index in excess of 15 $(\text{MPa})^{2/3}\text{m}^3/\text{Mg}$ and a strength of at least 100 MPa.
(Adapted from M. F. Ashby, *Materials Selection in Mechanical Design.* Copyright © 1992. Reprinted by permission of Butterworth-Heinemann Ltd.)

Materials cost is another important consideration in the selection process. In real-life engineering situations, economics of the application is often the overriding issue and normally will dictate the material of choice. One way to determine materials cost is by taking the product of the price (on a per-unit mass basis) and the required mass of material.

Cost considerations for these five candidate materials—steel, aluminum, and titanium alloys, and two engineering composites—are presented in Table CS1.2. In the first column is tabulated $\rho/\tau_f^{2/3}$. The next column lists the approximate relative cost, denoted

Table CS1.1 Density (ρ), Strength (τ_f), and Strength Performance Index (P) for Five Engineering Materials

Material	ρ (Mg/m^3)	τ_f (MPa)	$\tau_f^{2/3}/\rho = P$ $[(MPa)^{2/3}\ m^3/Mg]$
Carbon fiber–reinforced composite (0.65 fiber fraction)[a]	1.5	1140	72.8
Glass fiber–reinforced composite (0.65 fiber fraction)[a]	2.0	1060	52.0
Aluminum alloy (2024-T6)	2.8	300	16.0
Titanium alloy (Ti-6Al-4V)	4.4	525	14.8
4340 Steel (oil-quenched and tempered)	7.8	780	10.9

[a]The fibers in these composites are continuous, aligned, and wound in a helical fashion at a 45° angle relative to the shaft axis.

as $\bar{c}$; this parameter is simply the per-unit mass cost of material divided by the per-unit mass cost for low-carbon steel, one of the common engineering materials. The underlying rationale for using $\bar{c}$ is that although the price of a specific material will vary over time, the price ratio between that material and another will most likely change more slowly.

Finally, the right-hand column of Table CS1.2 shows the product of $\bar{c}$ and $\rho/\tau_f^{2/3}$. This product provides a comparison of the materials on the basis of the cost of materials for a cylindrical shaft that would not fracture in response to the twisting moment M_t. We use this product inasmuch as $\rho/\tau_f^{2/3}$ is proportional to the mass of material required (Equation CS1.8) and $\bar{c}$ is the relative cost on a per-unit mass basis. Now the most economical is the 4340 steel, followed by 2024-T6 aluminum, the glass fiber–reinforced composite, the carbon fiber–reinforced composite, and the titanium alloy. Thus, when the issue of economics is considered, there is a significant alteration within the ranking scheme. For example, inasmuch as the carbon fiber–reinforced composite is relatively expensive, it is significantly less desirable; in other words, the higher cost of this material may not outweigh the enhanced strength it provides.

Table CS1.2 Tabulation of the $\rho/\tau_f^{2/3}$ Ratio, Relative Cost ($\bar{c}$), and Product of $\rho/\tau_f^{2/3}$ and $\bar{c}$ for Five Engineering Materials[a]

Material	$\rho/\tau_f^{2/3}$ $\{10^{-2}[Mg/(MPa)^{2/3}m^3]\}$	$\bar{c}$ ($/$)	$\bar{c}(\rho/\tau_f^{2/3})$ $\{10^{-2}(\$/\$)[Mg/(MPa)^{2/3}m^3]\}$
4340 Steel (oil-quenched and tempered)	9.2	2.0	18
Aluminum alloy (2024-T6)	6.2	5.8	36
Glass fiber–reinforced composite (0.65 fiber fraction)[b]	1.9	53.0	101
Carbon fiber–reinforced composite (0.65 fiber fraction)[b]	1.4	99.4	139
Titanium alloy (Ti-6Al-4V)	6.8	35.3	240

[a]The relative cost is the ratio of the price per unit mass of the material and a low-carbon steel.

[b]The fibers in these composites are continuous, aligned, and wound in a helical fashion at a 45° angle relative to the shaft axis.

CS1.3 OTHER PROPERTY CONSIDERATIONS AND THE FINAL DECISION

To this point in our materials selection process, we have considered only the strength of materials. Other properties relative to the performance of the cylindrical shaft may be important—for example, stiffness, and, if the shaft rotates, fatigue behavior. Furthermore, fabrication costs should also be considered; in our analysis, they have been neglected.

Relative to stiffness, a stiffness-to-mass performance analysis similar to the one just discussed could be conducted. For this case, the stiffness performance index P_s is

$$P_s = \frac{\sqrt{G}}{\rho} \tag{CS1.11}$$

where G is the shear modulus. The appropriate materials selection chart (log G versus log ρ) would be used in the preliminary selection process. Subsequently, performance index and per-unit-mass cost data would be collected on specific candidate materials; from these analyses, the materials would be ranked on the basis of stiffness performance and cost.

In deciding on the best material, it may be worthwhile to make a table employing the results of the various criteria that were used. The tabulation would include, for all candidate materials, performance index, cost, and so forth for each criterion, as well as comments relative to any other important considerations. This table puts in perspective the important issues and facilitates the final decision process.

SUMMARY

- For a torsionally stressed cylindrical shaft, an expression for strength performance index was derived (Equation CS1.9).
- Using the appropriate materials selection chart (log strength versus log density, Figure CS1.3), a preliminary candidate search was conducted. From the results of this search, several candidate engineering materials were ranked on both strength-per-unit mass and cost bases.

REFERENCES

Ashby, M. F., *Materials Selection in Mechanical Design*, 4th edition, Butterworth-Heinemann, Oxford, UK, 2010.

Ashby, M. F., H. Shercliff, and D. Cebon, *Materials: Engineering, Science, Processing and Design*, 3rd edition, Butterworth-Heinemann, Oxford, UK, 2014.

Farag, M. M., *Materials and Process Selection for Engineering Design*, 3rd edition, CRC Press, Boca Raton, FL, 2014.

DESIGN PROBLEMS

CS1.D1 **(a)** Using the procedure outlined in this case study, ascertain which of the metal alloys listed in Appendix B (of the print textbook) have torsional strength performance indices greater than 10.0 (for τ_f and ρ in units of MPa and g/cm^3, respectively) and, in addition, shear strengths greater than 350 MPa.

(b) Also, using the cost database in Appendix C of the print textbook, conduct a cost analysis in the same manner as in this case study. For those materials that satisfy the criteria noted in part (a), and on the basis of this cost analysis, which material would you select for a solid cylindrical shaft? Why?

CS1.D2 Perform a stiffness-to-mass performance analysis on a solid cylindrical shaft that is subjected to a torsional stress. Use the same engineering materials that are listed in Table CS1.1. In addition, conduct a material cost analysis.

Rank these materials on the basis of both mass of material required and material cost. For glass and carbon fiber–reinforced composites, assume that the shear moduli are 8.6 and 9.2 GPa, respectively.

CS1.D3 (a) A cylindrical cantilever beam is subjected to a force F, as indicated in the accompanying figure. Derive strength and stiffness performance index expressions analogous to Equations CS1.9 and CS1.11 for this beam. The stress imposed on the unfixed end σ is

$$\sigma = \frac{FLr}{I} \qquad \text{(CS1.12)}$$

L, r, and I are, respectively, the length, radius, and moment of inertia of the beam. Furthermore, the beam-end deflection δ is

$$\delta = \frac{FL^3}{3EI} \qquad \text{(CS1.13)}$$

where E is the modulus of elasticity of the beam.

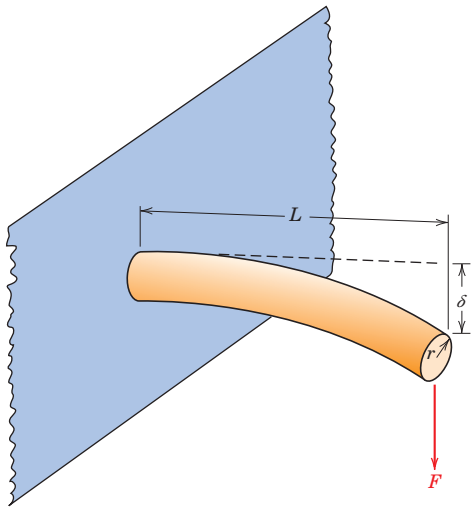

(b) From the properties database presented in Appendix B of the print textbook, select the metal alloys with stiffness performance indices greater than 3.0 (for E and ρ in units of GPa and g/cm^3, respectively).

(c) Also, using the cost database, Appendix C conduct a cost analysis in the same manner as in this case study. Relative to this analysis and that in part (b), which alloy would you select on a stiffness-per-mass basis?

(d) Now select the metal alloys with strength performance indices greater than 14.0 (for σ_y and ρ in units of MPa and g/cm^3, respectively), and rank them from highest to lowest P.

(e) Using the cost database, rank the materials in part (d) from least to most costly. Relative to this analysis and that in part (d), which alloy would you select on a strength-per-mass basis?

(f) Which material would you select if both stiffness and strength are to be considered relative to this application? Justify your choice.

CS1.D4 (a) Using the expression developed for stiffness performance index in Problem CS1.D3(a) and data contained in Appendix B (of the print textbook), determine stiffness performance indices for the following polymeric materials: high-density polyethylene, polypropylene, poly(vinyl chloride), polystyrene, polycarbonate, poly(methyl methacrylate), poly(ethylene terephthalate), polytetrafluoroethylene, and nylon 6,6. How do these values compare with those of the metallic materials? (*Note:* In Appendix B, where ranges of values are given, use average values.)

(b) Now, using the cost database in Appendix C (of the print textbook), conduct a cost analysis in the same manner as the case study. Use cost data for the raw forms of these polymers.

(c) Using the expression developed for strength performance index in Problem CS1.D3(a) and data contained in Appendix B, determine strength performance indices for these same polymeric materials.

CS1.D5 (a) A bar specimen having a square cross section of edge length c is subjected to a uniaxial tensile force F, as shown in the accompanying figure. Derive strength and stiffness performance index expressions analogous to Equations CS1.9 and CS1.11 for this bar.

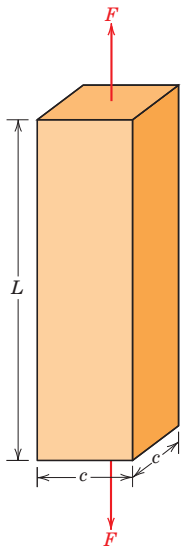

(b) From the properties database presented in Appendix B (of the print textbook), select the metal alloys with stiffness performance indices greater than 26.0 (for E and ρ in units of GPa and g/cm^3, respectively).

(c) Also, using the cost database in Appendix C (of the print textbook), conduct a cost analysis in the same manner as in this case study. Relative to this analysis and that in part (b), which alloy would you select on a stiffness-per-mass basis?

(d) Now select the metal alloys with strength performance indices greater than 120 (for σ_y and ρ in units of MPa and g/cm^3, respectively), and rank them from highest to lowest P.

(e) Using the cost database, rank the materials in part (d) from least to most costly. Relative to this analysis and that in part (d), which alloy would you select on a strength-per-mass basis?

(f) Which material would you select if both stiffness and strength are to be considered relative to this application? Justify your choice.

CS1.D6 Consider the plate shown in the accompanying figure that is supported at its ends and subjected to a force F that is uniformly distributed over the upper face as indicated. The deflection δ at the $L/2$ position is given by the expression

$$\delta = \frac{5FL^3}{32Ewt^3} \qquad \text{(CS1.14)}$$

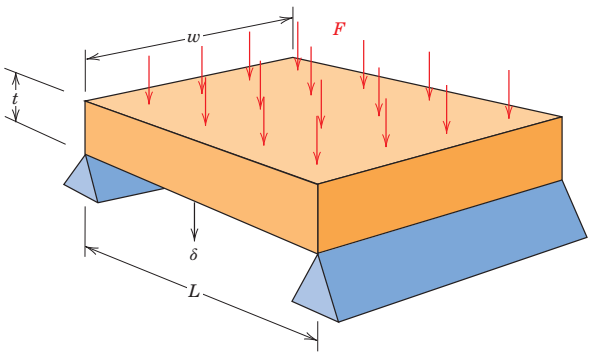

Furthermore, the tensile stress at the underside and also at the $L/2$ location is equal to

$$\sigma = \frac{3FL}{4wt^2} \qquad \text{(CS1.15)}$$

(a) Derive stiffness and strength performance index expressions analogous to Equations CS1.9 and CS1.11 for this plate. (*Hint:* Solve for t in these two equations, and then substitute the resulting expressions into the mass equation, as expressed in terms of density and plate dimensions.)

(b) From the properties database in Appendix B (of the print textbook), select the metal alloys with stiffness performance indices greater than 1.40 (for E and ρ in units of GPa and g/cm^3, respectively).

(c) Also, using the cost database in Appendix C (of the print textbook), conduct a cost analysis in the same manner as in this case study. Relative to this analysis and that in part (b), which alloy would you select on a stiffness-per-mass basis?

(d) Now select the metal alloys with strength performance indices greater than 5.0 (for σ_y and ρ in units of MPa and g/cm^3, respectively), and rank them from highest to lowest P.

(e) Using the cost database, rank the materials in part (d) from least to most costly. Relative to this analysis and that in part (d), which alloy would you select on a strength-per-mass basis?

(f) Which material would you select if both stiffness and strength are to be considered relative to this application? Justify your choice.

Case Study 2 Automobile Valve Spring

Learning Objective

After studying this case study, you should be able to do the following:

Briefly describe the steps that are used to ascertain whether a particular metal alloy is suitable for use in an automobile valve spring.

CS2.1 INTRODUCTION

The following case study discusses the valve spring found in a typical automobile engine. Issues addressed include mechanics of the deformation of helical springs, constraints imposed on the deformation of a typical valve spring, and, in addition, one of the steel alloys that is commonly used for these springs and the rationale for its use.

CS2.2 MECHANICS OF SPRING DEFORMATION

The basic function of a spring is to store mechanical energy as it is initially elastically deformed and then recoup this energy at a later time as the spring recoils. In this section helical springs that are used in mattresses and in retractable pens and as suspension springs in automobiles are discussed. A stress analysis will be conducted on this type of spring, and the results will then be applied to a valve spring that is used in automobile engines.

Consider the helical spring shown in Figure CS2.1, which has been constructed of wire having a circular cross section of diameter d; the coil center-to-center diameter is denoted as D. The application of a compressive force F causes a twisting force, or moment, denoted T, as shown in the figure. A combination of shear stresses results, the sum of which, τ, is

$$\tau = \frac{8FD}{\pi d^3} K_w \tag{CS2.1}$$

where K_w is a force-independent constant that is a function of the D/d ratio:

$$K_w = 1.60\left(\frac{D}{d}\right)^{-0.140} \tag{CS2.2}$$

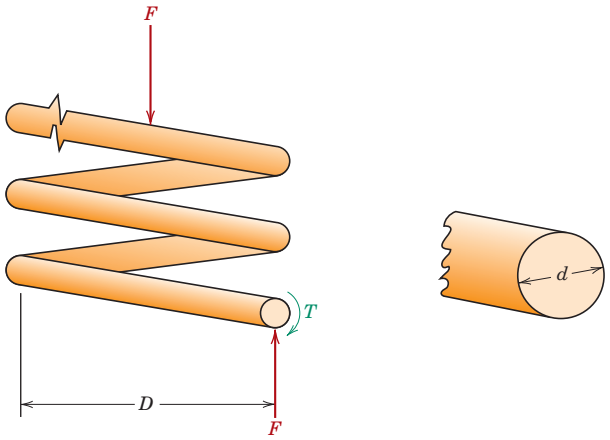

Figure CS2.1 Schematic diagram of a helical spring showing the twisting moment T that results from the compressive force F.
(Adapted from K. Edwards and P. McKee, *Fundamentals of Mechanical Component Design*. Copyright © 1991 by McGraw-Hill, Inc. Reproduced with permission of The McGraw-Hill Companies.)

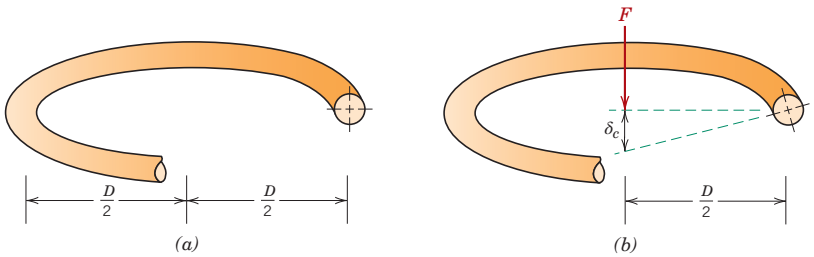

Figure CS2.2 Schematic diagrams of one coil of a helical spring, (*a*) prior to being compressed, and (*b*) showing the deflection δ_c produced from the compressive force F.
(Adapted from K. Edwards and P. McKee, *Fundamentals of Mechanical Component Design*. Copyright © 1991 by McGraw-Hill, Inc. Reproduced with permission of The McGraw-Hill Companies.)

Substitution of Equation CS2.2 into Equation CS2.1 leads to the following expression:

$$\tau = \frac{8FD}{\pi d^3}\left[1.60\left(\frac{D}{d}\right)^{-0.140}\right] \tag{CS2.3}$$

In response to the force F, the coiled spring will experience deflection, which will be assumed to be totally elastic. The amount of deflection per coil of spring, δ_c, as indicated in Figure CS2.2, is given by the expression

$$\delta_c = \frac{8FD^3}{d^4G} \tag{CS2.4}$$

where G is the shear modulus of the material from which the spring is constructed. Furthermore, δ_c may be computed from the total spring deflection, δ_s, and the number of effective spring coils, N_c, as

$$\delta_c = \frac{\delta_s}{N_c} \tag{CS2.5}$$

Now, solving for F in Equation CS2.4 gives

$$F = \frac{d^4\delta_c G}{8D^3} \tag{CS2.6}$$

and substitution of this expression for F into Equation CS2.3 leads to

$$\tau = \frac{\delta_c G d}{\pi D^2}\left[1.60\left(\frac{D}{d}\right)^{-0.140}\right] \tag{CS2.7}$$

Condition for nonpermanent spring deformation—shear yield strength and its relationship to shear modulus, number of effective coils, and spring and wire diameters

Under normal circumstances, it is desired that a spring experience no permanent deformation upon loading; this means that the right-hand side of Equation CS2.7 must be less than the shear yield strength τ_y of the spring material, or

$$\tau_y > \frac{\delta_c G d}{\pi D^2}\left[1.60\left(\frac{D}{d}\right)^{-0.140}\right] \tag{CS2.8}$$

CS2.3 VALVE SPRING DESIGN AND MATERIAL REQUIREMENTS

We shall now apply the results of the preceding section to an automobile valve spring. A cut-away schematic diagram of an automobile engine showing these springs is presented in Figure CS2.3. Functionally, springs of this type permit both intake and exhaust valves to alternately open and close as the engine is in operation. Rotation of the camshaft causes a valve to open and its spring to be compressed, so that the load on the spring is

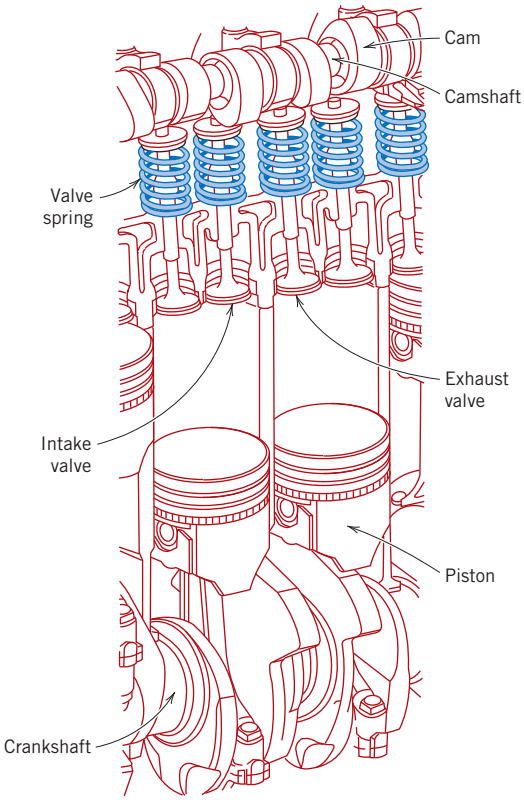

Figure CS2.3 Cut-away drawing of a section of an automobile engine in which various components including valves and valve springs are shown.

increased. The stored energy in the spring then forces the valve to close as the camshaft continues its rotation. This process occurs for each valve for each engine cycle, and over the lifetime of the engine it occurs many millions of times. Furthermore, during normal engine operation the temperature of the springs is approximately 80°C (175°F).

A photograph of a typical valve spring is shown in Figure CS2.4. The spring has a total length of 1.67 in. (42 mm), is constructed of wire having a diameter d of 0.170 in. (4.3 mm), has six coils (only four of which are active), and has a center-to-center diameter D

Figure CS2.4 Photograph of a typical automobile valve spring.

of 1.062 in. (27 mm). Furthermore, when installed and when a valve is completely closed, its spring is compressed a total of 0.24 in. (6.1 mm), which, from Equation CS2.4, gives an installed deflection per coil δ_{ic} of

$$\delta_{ic} = \frac{0.24 \text{ in.}}{4 \text{ coils}} = 0.060 \text{ in./coil } (1.5 \text{ mm/coil})$$

The cam lift is 0.30 in. (7.6 mm), which means that when the cam completely opens a valve, the spring experiences a maximum total deflection equal to the sum of the valve lift and the compressed deflection, namely, 0.30 in. + 0.24 in. = 0.54 in. (13.7 mm). Hence, the maximum deflection per coil, δ_{mc}, is

$$\delta_{mc} = \frac{0.54 \text{ in.}}{4 \text{ coils}} = 0.135 \text{ in./coil } (3.4 \text{ mm/coil})$$

Thus, we have available all of the parameters in Equation CS2.7 (taking $\delta_{ic} = \delta_{mc}$), except for τ_y, the required shear yield strength of the spring material.

However, the material parameter of interest for this valve spring is not the shear yield strength τ_y—rather, because the stress on the spring is continually cycled as the valve opens and closes during engine operation, it is necessary to design against the possibility of failure by fatigue. In this regard, we want to choose a metal alloy that has a fatigue limit greater than the cyclic stress amplitude to which the spring is subjected. For this reason, steel alloys that have fatigue limits are normally used for valve springs.

Computation of Shear Stress Amplitude

The shear stress amplitude for this valve spring τ_a may be computed using the following equation:[5]

$$\tau_a = \frac{\tau_{\max} - \tau_{\min}}{2} \tag{CS2.9}$$

In this expression $\tau_{\max}$ and $\tau_{\min}$ are the maximum and minimum shear stresses to which the spring is subjected; their values may be determined using Equation CS2.7. For $\tau_{\max}$ we take δ_c to be the maximum value—that is, δ_{mc}, which is equal to 0.135 in. as noted above. A shear modulus G of 11.5×10^6 psi (79 GPa) will be assumed—the typical value for most steel alloys; furthermore, it is also valid at the 80°C service temperature. Thus, $\tau_{\max}$ is computed as follows:

$$\tau_{\max} = \frac{\delta_{mc} G d}{\pi D^2}\left[1.60\left(\frac{D}{d}\right)^{-0.140}\right] \tag{CS2.10}$$

$$= \left[\frac{(0.135 \text{ in.})(11.5 \times 10^6 \text{ psi})(0.170 \text{ in.})}{(\pi)(1.062 \text{ in.}^2)}\right]\left[1.60\left(\frac{1.062}{0.170}\right)^{-0.140}\right]$$

$$= 92{,}200 \text{ psi } (635 \text{ MPa})$$

Likewise, $\tau_{\min}$ is determined taking $\delta_c = \delta_{ic} = 0.060$ in.:

$$\tau_{\min} = \frac{\delta_{ic} G d}{\pi D^2}\left[1.60\left(\frac{D}{d}\right)^{-0.140}\right] \tag{CS2.11}$$

$$= \left[\frac{(0.060 \text{ in.})(11.5 \times 10^6 \text{ psi})(0.170 \text{ in.})}{(\pi)(1.062 \text{ in.}^2)}\right]\left[1.60\left(\frac{1.062}{0.170}\right)^{-0.140}\right]$$

$$= 41{,}000 \text{ psi} (280 \text{ MPa})$$

[5]Equation CS2.9 is the shear-stress equivalent of the tension-compression stress amplitude equation found in the Cyclic Stresses section of the print textbook.

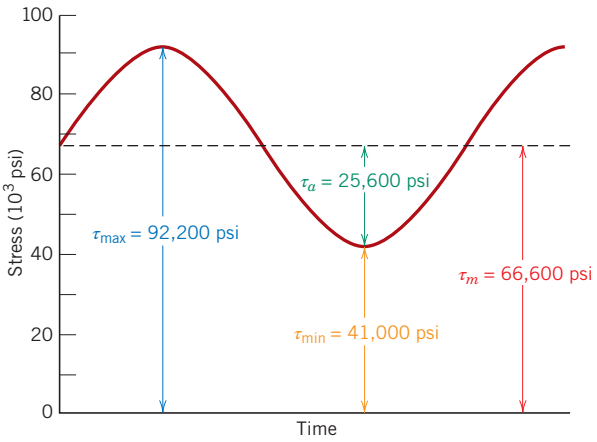

Figure CS2.5 Shear stress versus time for an automobile valve spring.

It is now possible to compute the shear stress amplitude on the spring using Equation CS2.9—that is,

$$\begin{aligned}\tau_a &= \frac{\tau_{max} - \tau_{min}}{2} \\ &= \frac{92{,}200 \text{ psi} - 41{,}000 \text{ psi}}{2} \\ &= 25{,}600 \text{ psi } (177 \text{ MPa})\end{aligned}$$

The variation of shear stress with time for this valve spring is noted in Figure CS2.5; the time axis is not scaled, inasmuch as the time scale will depend on engine speed.

Fatigue Limit Computation

The following procedure will be followed to determine the fatigue limit for a steel alloy commonly used for automobile valve springs:

1. The fatigue limit for steel alloys exposed to reversed stress cycling will be given.
2. An expression will be presented that may be used for fatigue limit extrapolations when stress cycles are not reversed.
3. Finally, the fatigue limit will be computed for the specific alloy.

For steel alloys used in spring design, and for reversed stress cycling—that is, $\tau_m = 0$, where τ_m is the mean stress—the fatigue limit (expressed as stress amplitude) is 45,000 psi (310 MPa); furthermore, the fatigue limit threshold occurs at about 10^6 cycles. The *S-N* diagram for these steels would appear as shown in Figure CS2.6.[6]

This situation is complicated by the fact that the stress cycle is not completely reversed (i.e., $\tau_m \neq 0$ or $\tau_{max} \neq -\tau_{min}$). Between minimum and maximum shear stresses the spring remains in compression; as noted earlier, δ_{ic} and δ_{mc} are both compressive deflections. This means that this 45,000-psi (310-MPa) fatigue limit is not valid, and we must compute a new value, which is possible by making an extrapolation. If the stress amplitude is significantly below this extrapolated limit, then the spring design is satisfactory.

[6]For an automobile that travels 100,000 miles (161,000 km), the number of cycles its valve springs experience is greater than 10^8. Thus, we may use the fatigue limit as the design stress inasmuch as the limit threshold (viz. 10^6 cycles) is exceeded.

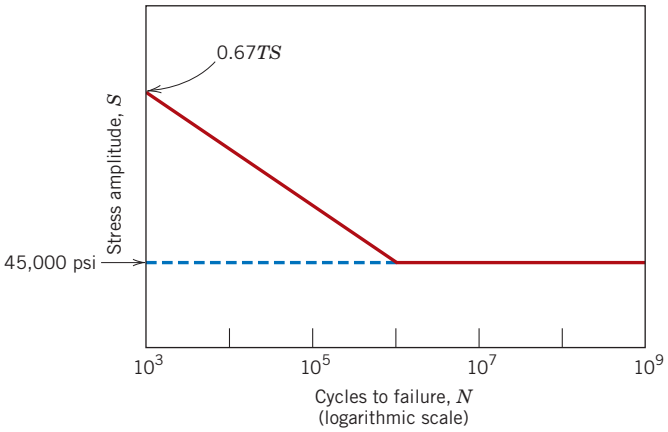

Figure CS2.6 Shear stress amplitude versus logarithm of the number of cycles to fatigue failure for typical ferrous alloys.

A reasonable fatigue-limit extrapolation for this $\tau_m \neq 0$ situation may be made using the following expression (known as the Goodman equation):

$$\tau_f = \tau_{f_0}\left(1 - \frac{\tau_m}{0.67TS}\right) \tag{CS2.12}$$

Here τ_f is the fatigue limit for the mean stress τ_m; τ_{f_0} is the fatigue limit for $\tau_m = 0$ [i.e., 45,000 psi (310 MPa)]; also TS is the tensile strength of the alloy. To determine the new fatigue limit τ_f from this expression necessitates the computation of both the mean stress for the spring (τ_m) and tensile strength of the alloy (TS).

Computation of the means stress τ_m is possible using the following equation:[7]

$$\tau_m = \frac{\tau_{\max} + \tau_{\min}}{2} \tag{CS2.13}$$

Minimum and maximum shear stresses were computed above [viz., $\tau_{\min} = 41{,}000$ psi (280 MPa) and $\tau_{\max} = 92{,}200$ psi (635 MPa)]. Therefore, the mean stress is equal to

$$\begin{aligned}\tau_m &= \frac{41{,}000 \text{ psi} + 92{,}200 \text{ psi}}{2} \\ &= 66{,}600 \text{ psi (460 MPa)}\end{aligned}$$

This mean stress is also noted in the plot of Figure CS2.5.

At this point we compute the tensile strength of a steel alloy commonly used for springs—viz., an ASTM 232 chrome–vanadium steel that has a composition of 0.48–0.53 wt% C, 0.80–1.10 wt% Cr, a minimum of 0.15 wt% V, and the balance being Fe. Spring wire is normally cold drawn to the desired diameter; consequently, the wire will strain harden and tensile strength will increase with the amount of drawing (i.e., as the diameter decreases). For this alloy, it has been experimentally verified that, for the diameter d in inches, the tensile strength is equal to

$$TS \text{ (psi)} = (169{,}000)(d)^{-0.167} \tag{CS2.14}$$

Since $d = 0.170$ in. for this valve spring, then

$$\begin{aligned}TS \text{ (psi)} &= (169{,}000)(0.170 \text{ in.})^{-0.167} \\ &= 227{,}200 \text{ psi (1570 MPa)}\end{aligned}$$

[7]Equation CS2.13 is the shear-stress equivalent of the tension-compression mean stress equation found in the Cyclic Stresses section of the print textbook.

It is now possible to compute the fatigue limit for this chrome-vanadium steel using Equation CS2.12 with

$$\tau_{f_0} = 45{,}000 \text{ psi}$$
$$\tau_m = 66{,}600 \text{ psi}$$
$$TS = 227{,}200 \text{ psi}$$

Thus

$$\begin{aligned}\tau_f &= \tau_{f_0}\left(1 - \frac{\tau_m}{0.67TS}\right) \\ &= (45{,}000 \text{ psi})\left[1 - \frac{66{,}600 \text{ psi}}{(0.67)(227{,}200 \text{ psi})}\right] \\ &= 25{,}300 \text{ psi } (175 \text{ MPa})\end{aligned}$$

In summary, this fatigue limit is slightly less than the stress amplitude of the spring determined above [i.e., τ_f (25,300 psi) $<$ τ_a (25,600 psi)], which means that this spring design is not satisfactory.

The fatigue limit of this alloy may be increased to greater than 25,300 psi (175 MPa) by shot peening, a procedure described in the Factors That Affect Fatigue section found in the Failure chapter of the print textbook. Shot peening involves the introduction of residual compressive surface stresses by plastically deforming outer surface regions; small and very hard particles are projected onto the surface at high velocities. This is an automated procedure commonly used to improve the fatigue resistance of valve springs; in fact, the spring shown in Figure CS2.4 has been shot peened, which accounts for its rough surface texture. Shot peening has been observed to increase the fatigue limit of steel alloys in excess of 50% and, in addition, to significantly reduce the degree of scatter of fatigue data.

This spring design, including shot peening, may be satisfactory; however, its adequacy should be verified by experimental testing. The testing procedure is relatively complicated and, consequently, will not be discussed in detail. In essence, it involves performing a relatively large number of fatigue tests (on the order of 1000) on this shot-peened ASTM 232 steel, in shear, using a mean stress of 66,600 psi (460 MPa) and a stress amplitude of 25,600 psi (177 MPa), and for 10^6 cycles. On the basis of the number of failures, an estimate of the survival probability can be made. For the sake of argument, let us assume that this probability turns out to be 0.99999; this means that one spring in 100,000 produced will fail.

Suppose you are employed by one of the large automobile companies that manufactures on the order of 1 million cars per year, and that the engine powering each automobile is a six-cylinder one. Since for each cylinder there are two valves, and thus two valve springs, a total of 12 million springs would be produced every year. For the preceding survival probability rate, the total number of spring failures would be approximately 120, which also corresponds to 120 engine failures. As a practical matter, one would have to weigh the cost of replacing these 120 engines against the cost of a spring redesign.

Redesign options would involve taking measures to reduce the shear stresses on the spring by altering the parameters in Equation CS2.7. This would include either (1) increasing the coil diameter D, which would also necessitate increasing the wire diameter d, or (2) increasing the number of coils N_c.

SUMMARY

- A stress analysis was first performed on a helical spring, which was then extended to an automobile valve spring. Since the valve spring is subjected to cyclic loading, the possibility of fatigue failure is crucial to its performance.

- The results of this analysis included computation of the shear stress amplitude, the magnitude of which was almost identical to the calculated fatigue limit for a chrome–vanadium steel that is commonly used for valve springs. It was noted that the fatigue limit of valve springs is often enhanced by shot peening.
- Finally, a procedure was suggested for assessing the economic feasibility of this spring design incorporating the shot-peened chrome–vanadium steel.

REFERENCES

Budynas, R. G., and J. K. Nisbett, *Shigley's Mechanical Engineering Design,* 9th edition, McGraw-Hill, New York, NY, 2011.

Juvinall, R. C., and K. M. Marshek, *Fundamentals of Machine Component Design*, 5th edition, Chapter 12, Wiley, Hoboken, NJ, 2011.

SPREADSHEET PROBLEM

CS2.1SS Generate a spreadsheet that allows the user to specify the number of effective coils (N), the spring coil-to-coil diameter (D), the wire cross-section diameter (d), the fatigue limit (for $\tau_m = 0$) (τ_{f_0}), the tensile strength (TS), and the shear modulus (G), and calculates the fatigue limit (for $\tau_m \neq 0$) (τ_f) as well as the actual stress amplitude (τ_a) for an automobile valve spring. Incorporate into this routine values cited for installed and maximum deflections per coil (i.e., $\delta_{ic} = 0.24$ in. and $\delta_{mc} = 0.54$ in.).

DESIGN PROBLEMS

CS2.D1 A spring having a center-to-center diameter of 20 mm (0.8 in.) is to be constructed of cold-drawn and annealed 316 stainless steel wire that is 2.5 mm (0.10 in.) in diameter; this spring design calls for eight coils.

(a) What is the maximum tensile load that may be applied such that the total spring deflection will be no more than 6.5 mm (0.26 in.)?

(b) What is the maximum tensile load that may be applied without any permanent deformation of the spring wire? Assume that the shear yield strength is $0.6\sigma_y$, where σ_y is the yield strength in tension.

CS2.D2 You have been asked to select a material for a spring that is to be stressed in tension. It is to consist of ten coils, and the coil-to-coil diameter called for is 15 mm; furthermore, the diameter of the spring wire must be 2.0 mm. Upon application of a tensile force of 35 N, the spring is to experience a deflection of no more than 12 mm and not plastically deform.

(a) From the materials included in the database in Appendix B (in the print textbook), make a list of candidate materials that meet the preceding criteria. Assume that the shear yield strength is $0.6\sigma_y$, where σ_y is the yield strength in tension, and that the shear modulus is equal to $0.4E$, E being the modulus of elasticity.

(b) Now, from this list of candidate materials, select the one you would use for this spring application. In addition to the preceding criteria, the material must be relatively corrosion resistant and, of course, capable of being fabricated into wire form. Justify your decision.

CS2.D3 A spring having seven coils and a coil-to-coil diameter of 0.5 in. is to be made of cold-drawn steel wire. When a tensile load of 15 lb_f is applied, the spring is to deflect no more than 0.60 in. The cold-drawing operation will, of course, increase the shear yield strength of the wire, and it has been observed that τ_y (in ksi) depends on wire diameter d (in in.) according to

$$\tau_y = \frac{63}{d^{0.2}} \qquad \text{(CS2.15)}$$

If the shear modulus for this steel is 11.5×10^6 psi, calculate the minimum wire diameter required such that the spring will not plastically deform when subjected to the preceding load.

CS2.D4 A helical spring is to be constructed from a 4340 steel. The design calls for five coils, a coil-to-coil diameter of 12 mm, and a wire diameter of 3 mm. Furthermore, a maximum total deflection of 5.0 mm is possible without any plastic deformation. Specify a heat treatment for this 4340 steel wire in order for the spring to meet the preceding criteria. Assume a shear modulus of 80 GPa for this steel alloy and that $\tau_y = 0.6\sigma_y$. (*Note:* Heat treatment of the 4340 steel is discussed in the Tempered Martensite section found in the Phase Transformations chapter of the print textbook.)

Case Study 3 Failure of an Automobile Rear Axle[8]

Learning Objective

After studying this case study, you should be able to do the following:

1. Briefly describe the difference in surface features (as observed in scanning electron micrographs) for a steel alloy that (a) experienced a ductile fracture and (b) failed in a brittle manner.

CS3.1 INTRODUCTION

After an accident in which a light pickup truck left the road and overturned, it was noted that one of the rear axles had failed at a point near the wheel mounting flange. This axle was made of a steel that contained approximately 0.3 wt% C. Furthermore, the other axle was intact and did not experience fracture. An investigation was carried out to determine whether the axle failure caused the accident or whether the failure occurred as a consequence of the accident.

Figure CS3.1 is a schematic diagram that shows the components of a rear axle assembly of the type used in this pickup truck. The fracture occurred next to the bearing lock nut, as noted in this schematic. A photograph of one end of the failed axle shaft is presented in Figure CS3.2*a*, and Figure CS3.2*b* is an enlarged view of the other fractured piece that includes the wheel mounting flange and the stub end of the failed axle. Here (Figure CS3.2*b*) note that a keyway was present in the area of failure; furthermore, threads for the lock nut were also situated next to this keyway.

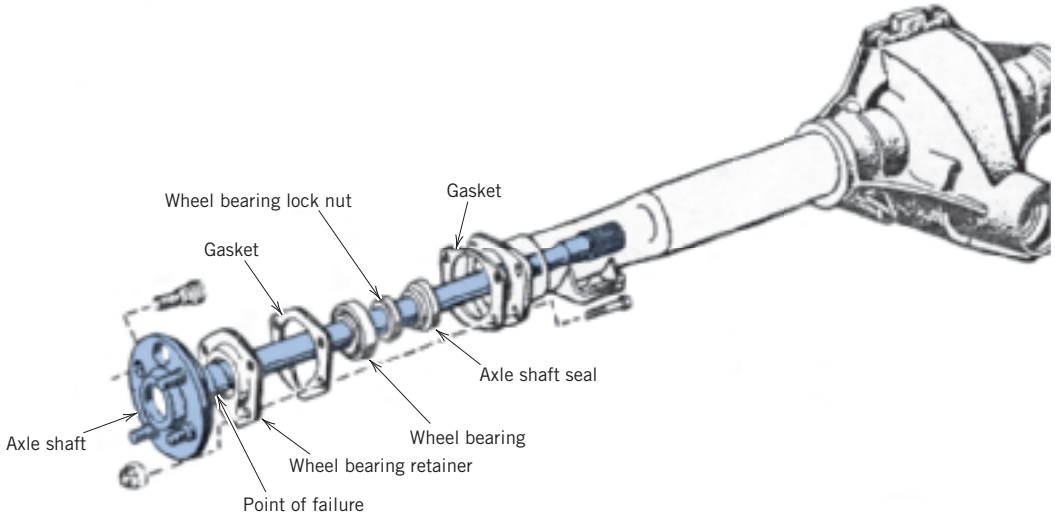

Figure CS3.1 Schematic diagram showing typical components of a light truck axle and the fracture site for the failed axle of this case study.
(Reproduced from *MOTOR Auto Repair Manual,* 39th edition, Copyright © 1975. By permission of the Hearst Corporation.)

[8]This case study was taken from Lawrence Kashar, "Effect of Strain Rate on the Failure Mode of a Rear Axle," *Handbook of Case Histories in Failure Analysis,* Vol. 1, pp. 74–78, ASM International, Materials Park, OH, 1992.

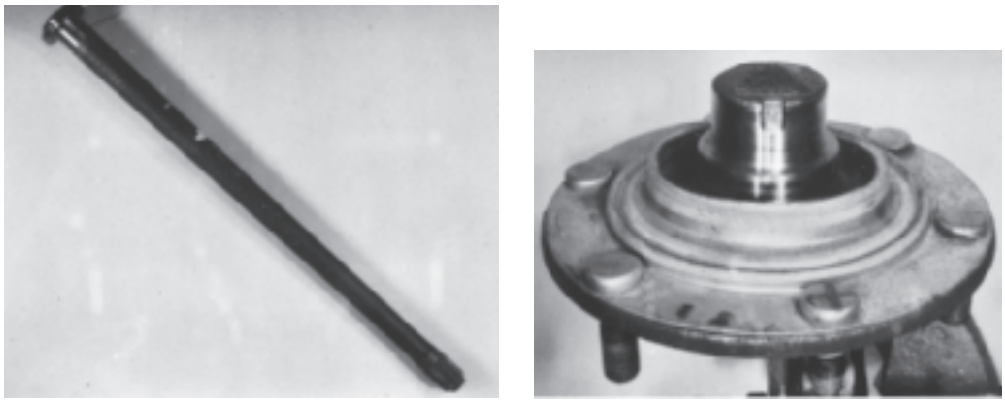

(a) (b)

Figure CS3.2 (*a*) Photograph of one section of the failed axle. (*b*) Photograph showing wheel mounting flange and stub end of failed axle.
[Reproduced with permission from *Handbook of Case Histories in Failure Analysis,* Vol. 1 (1992), ASM International, Materials Park, OH, 44073-0002.]

Upon examination of the fracture surface, it was noted that the region corresponding to the outside shaft perimeter [being approximately 6.4 mm (0.25 in.) wide] was very flat; furthermore, the center region was rough in appearance.

Thus, on the basis of these failed axle components it is necessary to design and conduct appropriate tests and procedures to determine

(1) if the accident caused the axle failure, or

(2) if the axle failure caused the accident.

We now discuss the analytical procedures that were used to make this determination.

CS3.2 TESTING PROCEDURE AND RESULTS

Details of the fracture surface in the vicinity of the keyway are shown in the photograph of Figure CS3.3; note that the keyway appears at the bottom of the photograph. Both the flat outer perimeter and rough interior regions may be observed in the photograph. There are chevron patterns that emanate inward from the corners of and parallel to

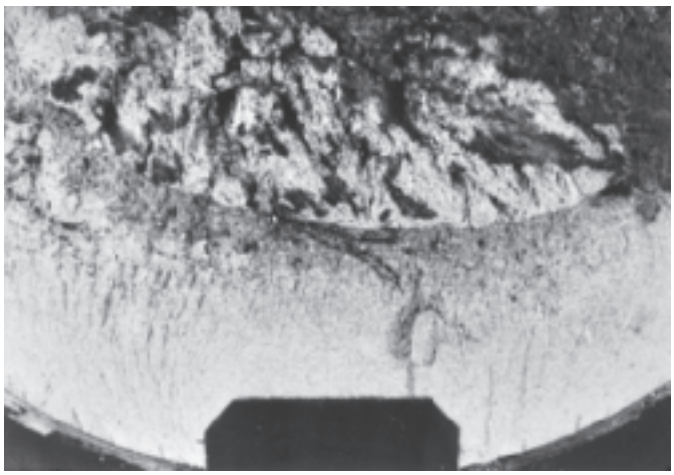

Figure CS3.3 Optical micrograph of failed section of axle that shows the keyway (bottom), as well as the flat outer-perimeter and rough core regions. [Reproduced with permission from *Handbook of Case Histories in Failure Analysis,* Vol. 1 (1992), ASM International, Materials Park, OH, 44073-0002.]

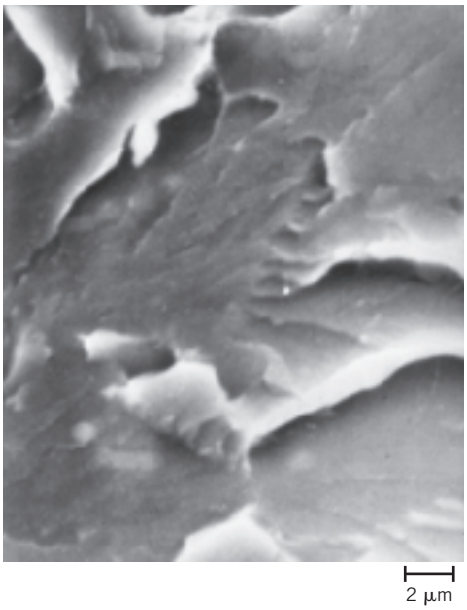

Figure CS3.4 Scanning electron micrograph of failed axle outer-perimeter region near the keyway, which shows cleavage features. 3500×.
[Reproduced with permission from *Handbook of Case Histories in Failure Analysis,* Vol. 1 (1992), ASM International, Materials Park, OH, 44073-0002.]

the sides of the keyway; these are barely discernible in the photograph but indicate the direction of crack propagation.

Fractographic analyses were also conducted on the fracture surface. Figure CS3.4 shows a scanning electron micrograph taken near one of the keyway corners. Cleavage features may be noted in this micrograph, whereas any evidence of dimples and fatigue striations is absent. These results indicate that the mode of fracture within this outer periphery of the shaft was brittle.

An SEM micrograph taken of the rough central region (Figure CS3.5) revealed the presence of brittle cleavage features and also dimples; thus, it is apparent that the failure mode in this central interior region was mixed—that is, it was a combination of both brittle and ductile fracture.

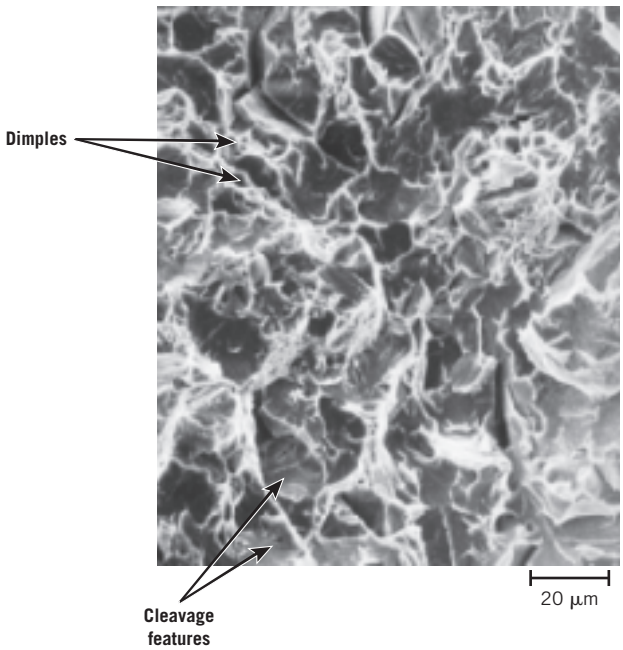

Figure CS3.5 Scanning electron micrograph of the failed axle rough core region, which is composed of mixed cleavage and dimpled regions. 570×.
[Reproduced with permission from *Handbook of Case Histories in Failure Analysis,* Vol. 1 (1992), ASM International, Materials Park, OH, 44073-0002.]

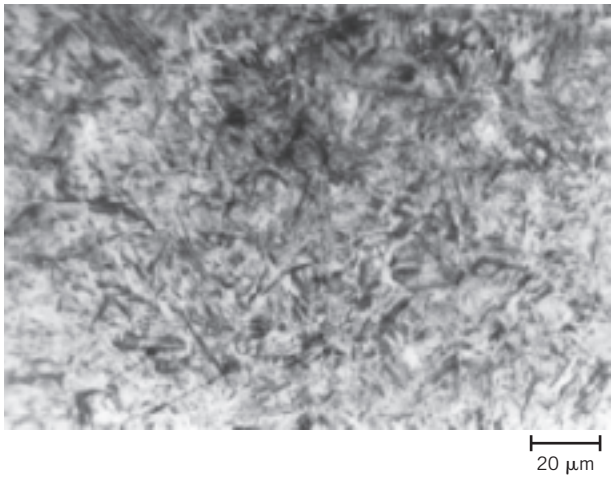

Figure CS3.6 Optical photomicrograph of the failed axle outer-perimeter region, which is composed of tempered martensite. 500×. [*Note:* Although the microstructure for tempered martensite in this figure appears to be different from that shown in the Tempered Martensite section found in the Phase Transformations chapter of the print textbook, they are nevertheless the same. One reason for this disparity in appearance is due to the difference in magnification of the micrographs: the electron micrograph in the print textbook is at a magnification that is approximately 20 times greater than this micrograph. Furthermore, the dark regions of this photomicrograph are clusters of Fe_3C particles (which are unresolved) that stand in relief above the etched α-ferrite matrix, which appears light.] [Reproduced with permission from *Handbook of Case Histories in Failure Analysis,* Vol. 1 (1992), ASM International, Materials Park, OH, 44073-0002.]

Metallographic examinations were also performed. A transverse cross section of the failed axle was polished, etched, and photographed using the optical microscope. The microstructure of the outer periphery region, as shown in Figure CS3.6, consisted of tempered martensite.[9] On the other hand, the microstructure in the central region was completely different per the photomicrograph of Figure CS3.7. It may be noted that the microconstituents are ferrite, pearlite, and possibly some bainite.[10] In addition, transverse microhardness measurements were taken along the cross section; Figure CS3.8 is a plot of the resulting hardness profile. Here it may be noted that the maximum hardness of approximately 56 HRC occurred near the surface, and that hardness diminished with radial distance to a hardness of about 20 HRC near the center. On the basis of the

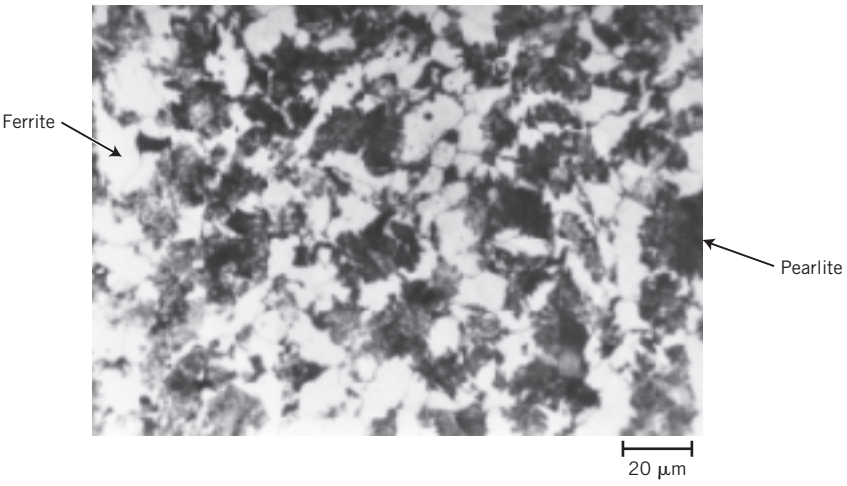

Figure CS3.7 Optical photomicrograph of the failed axle core region, which is composed of ferrite and pearlite (and possibly bainite). 500×. [Reproduced with permission from *Handbook of Case Histories in Failure Analysis,* Vol. 1 (1992), ASM International, Materials Park, OH, 44073-0002.]

[9] For a discussion of tempered martensite, see the Tempered Martensite section found in the Phase Transformations chapter of the print textbook.

[10] Ferrite, pearlite, and bainite microconstituents are discussed in the Isothermal Transformation Diagrams section found in the Phase Transformations chapter of the print textbook.

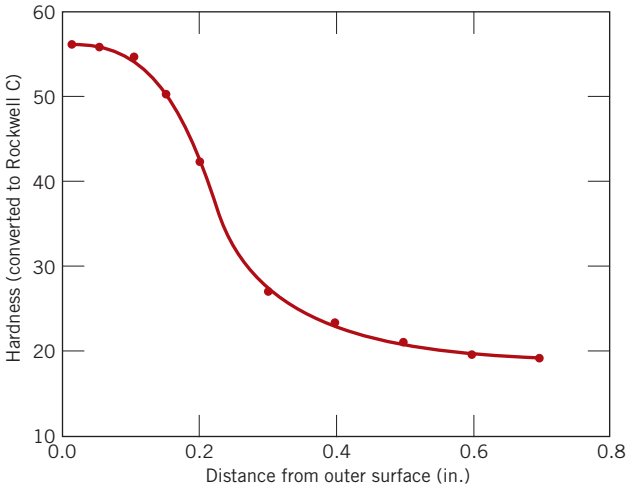

Figure CS3.8 Transverse hardness profile across the axle cross section. (Microhardness readings were converted to Rockwell C values). [Reproduced with permission from *Handbook of Case Histories in Failure Analysis,* Vol. 1 (1992), ASM International, Materials Park, OH, 44073-0002.]

observed microstructures and this hardness profile, it was assumed that the axle had been induction hardened.[11]

The results of these fractographic/metallographic analyses and hardness tests are summarized in Table CS3.1.

At this point in the investigation it was not possible to ascertain irrefutably whether the accident caused the axle failure (scenario 1) or whether the axle fracture caused the accident (scenario 2). The high hardness and, in addition, the evidence of cleavage of the outer surface layer indicated that this region failed in a brittle manner as a result of being overloaded (i.e., as a result of the accident, scenario 1). On the other hand, the evidence of a mixed ductile-brittle mode of fracture in the central region neither supported nor refuted either of these two failure scenarios.

Assuming the validity of the first scenario, it was hypothesized that the core region was strain-rate sensitive to fracture; that is, at high strain rates, as with the truck rollover, the fracture mode would be brittle. By contrast, if failure resulted from loads that were applied relatively slowly, as under normal driving conditions (the second scenario), the mode of failure would be more ductile.

In order to explore the feasibility of scenario 1 (i.e., the strain-rate sensitivity of the core region), it was decided to fabricate and test impact specimens taken from both outer-perimeter and core regions; in addition, a tension test was to be conducted on a core-region specimen. Failure surfaces for all three specimens were to be subjected to

Table CS3.1 Tabulation of Test Results on Specimens Taken from Failed Rear Truck Axle

Analytical Technique	*Result for Outer Region*	*Result for Core Region*
Fractographic	Cleavage features (brittle fracture)	Cleavage features/dimples (ductile/brittle fracture)
Metallographic	Tempered martensite	Ferrite, pearlite (bainite?)
Hardness tests (profile) (i.e., heat treatment)	Induction hardened	

[11]With induction hardening, the surface of a piece of medium-carbon steel is rapidly heated using an induction furnace. The piece is then quickly quenched so as to produce an outer surface layer of martensite (which is subsequently tempered), with a mixture of ferrite and pearlite at interior regions.

SEM examinations. The following results from these tests/examinations would be expected if the core region of the axle were sensitive to the rate of straining:

- The failure of the core-region specimen to be impact (high strain rate) tested would not be totally ductile in nature.
- The core-region specimen to be tensile (low strain rate) tested would display at least a moderate degree of ductility.
- The outer-perimeter specimen to be impact tested would fail in a totally brittle manner.

Impact Tests

For the impact tests, small [~2.5-mm- (0.1-in.-) wide] Charpy V-notch test specimens were prepared from both outer-perimeter and interior areas. Because the hardened outer region was very thin (6.4 mm thick), careful machining of these specimens was required. Impact tests were conducted at room temperature, and the energy absorbed by the surface specimen was significantly lower than for the core specimen [4 J (3 ft-lb_f) versus 11 J (8 ft-lb_f)]. Furthermore, the appearances of the fracture surfaces for the two specimens were dissimilar. Very little, if any, deformation was observed for the outer-perimeter specimen (Figure CS3.9); conversely, the core specimen deformed significantly (Figure CS3.10).

Fracture surfaces of these impact specimens were then subjected to examination using the SEM. Figure CS3.11, a micrograph of the outer-perimeter specimen that was impact tested, reveals the presence of cleavage features, which indicates that this was a brittle fracture. Furthermore, the morphology of this fracture surface is similar to that of the actual failed axle (Figure CS3.4).

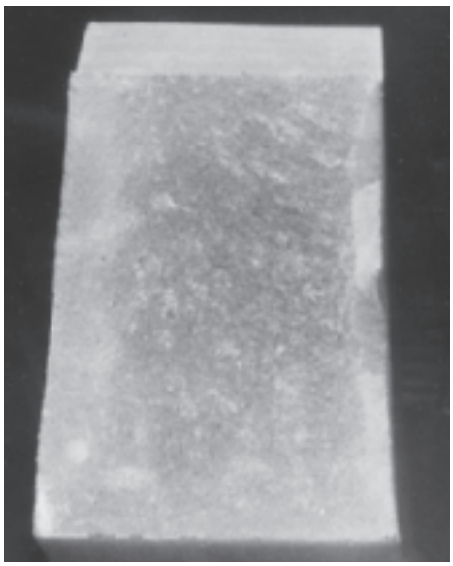

Figure CS3.9 Fracture surface of the Charpy impact specimen that was taken from the outer-perimeter region.
[Reproduced with permission from *Handbook of Case Histories in Failure Analysis,* Vol. 1 (1992), ASM International, Materials Park, OH, 44073-0002.]

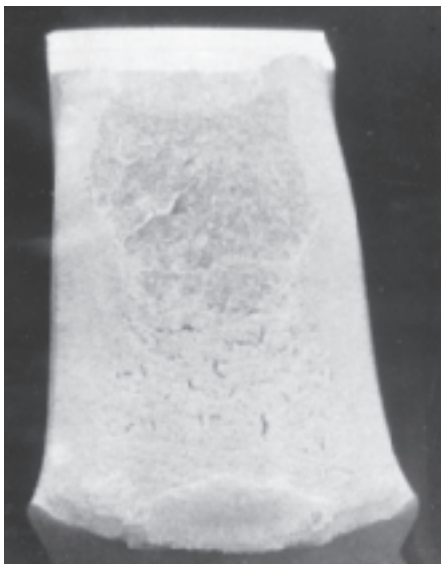

Figure CS3.10 Fracture surface of the Charpy impact specimen that was taken from the core region.
[Reproduced with permission from *Handbook of Case Histories in Failure Analysis,* Vol. 1 (1992), ASM International, Materials Park, OH, 44073-0002.]

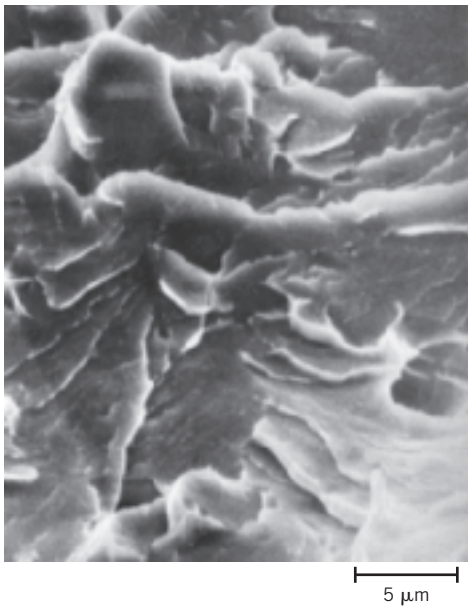

Figure CS3.11 Scanning electron micrograph of the fracture surface for the impact specimen prepared from the outer-perimeter region of the failed axle. 3000×. [Reproduced with permission from *Handbook of Case Histories in Failure Analysis,* Vol. 1 (1992), ASM International, Materials Park, OH, 44073-0002.]

For the impact specimen taken from the core region, the fracture surface had a much different appearance; Figures CS3.12*a* and CS3.12*b* show micrographs for this specimen, which were taken at relatively low and high magnifications, respectively. These micrographs reveal the details of this surface to be composed of interspersed cleavage features and shallow dimples, being similar to the failed axle, as shown in Figure CS3.5. Thus, the fracture of this specimen was of the mixed-mode type, having both ductile and brittle components.

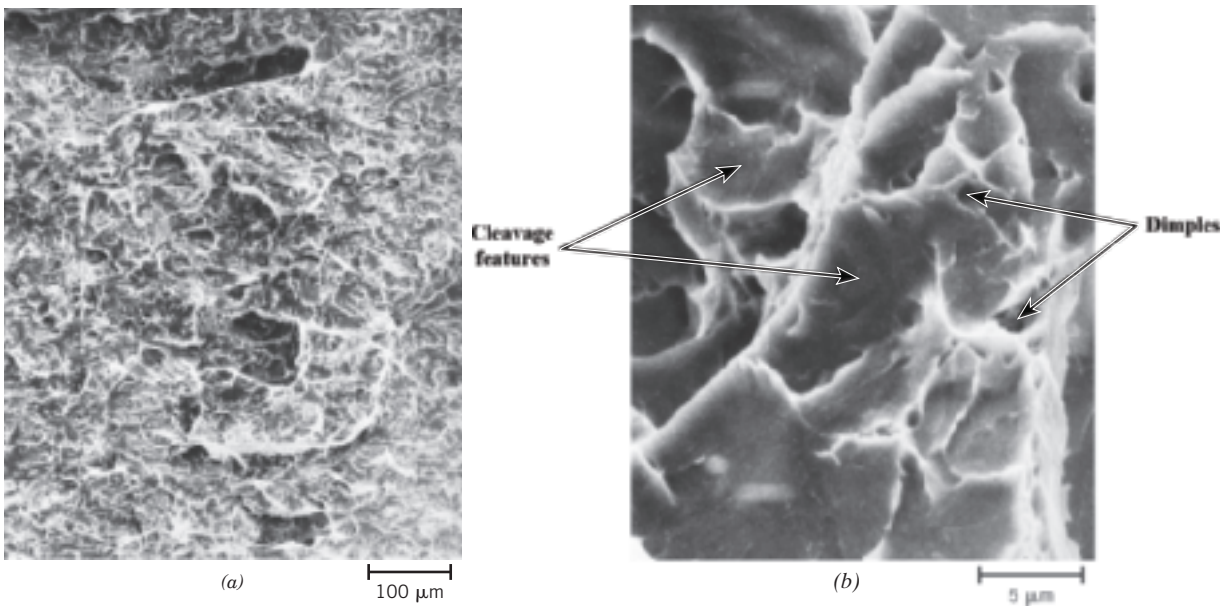

Figure CS3.12 (*a*) Scanning electron micrograph of the fracture surface for the impact specimen prepared from the core region of the failed axle. 120×. (*b*) Scanning electron micrograph of the fracture surface for the impact specimen prepared from the core region of the failed axle taken at a higher magnification than (*a*); interspersed cleavage and dimpled features may be noted. 3000×.
[Reproduced with permission from *Handbook of Case Histories in Failure Analysis,* Vol. 1 (1992), ASM International, Materials Park, OH, 44073-0002.]

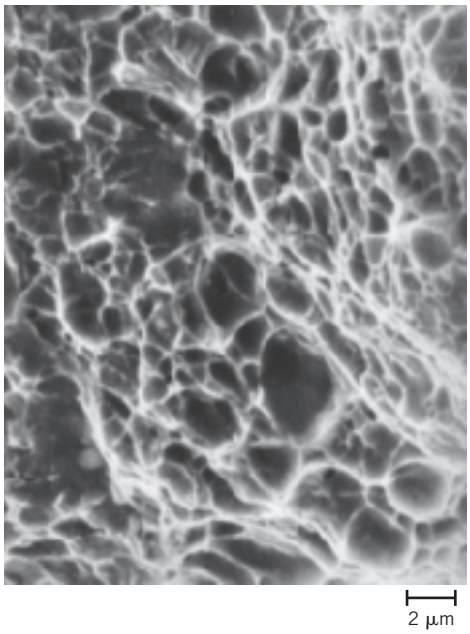

Figure CS3.13 Scanning electron micrograph of the fracture surface for the core specimen that was tensile tested; a completely dimpled structure may be noted. Approximately 3500×. [Reproduced with permission from *Handbook of Case Histories in Failure Analysis,* Vol. 1 (1992), ASM International, Materials Park, OH, 44073-0002.]

Tensile Test

A tensile specimen taken from the core region was pulled in tension to failure. The fractured specimen displayed the cup-and-cone configuration, which indicated at least a moderate level of ductility. A fracture surface was examined using the SEM, and its morphology is presented in the micrograph of Figure CS3.13. The surface was composed entirely of dimples, which confirms that this material was at least moderately ductile and that there was no evidence of brittle fracture. Thus, although this core material exhibited mixed-mode fracture under impact loading conditions, when the load was applied at a relatively slow rate (as with the tensile test), failure was highly ductile in nature.

A summary of these impact and tensile tests is presented in Table CS3.2.

CS3.3 DISCUSSION

In light of the previous discussion, it was supposed that the truck rollover was responsible for the axle failure (i.e., scenario 1 was valid). Reasons for this supposition are as follows (see Tables CS3.1 and CS3.2):

1. The outer-perimeter region of the failed axle shaft failed in a brittle manner, as did also the specimen taken from this region that was impact tested. This conclusion was based on the fact that both fracture surfaces were very flat and that SEM micrographs revealed the presence of cleavage facets.

Table CS3.2 Tabulation of Impact and Tension Test Results for Specimens Taken from Core and Outer Regions of Failed Truck Rear Axle

Specimen/Test	*Fracture Mode*	*Fractographic Features*
Core region/impact	Some ductility	Dimples and cleavage features
Outer region/impact	Brittle	Cleavage features
Core region/tension	Ductile	Dimples

2. The fracture behavior of the core region was strain-rate sensitive and indicated that axle failure was due to a single high-strain-rate incident. Fracture surface features for both the failed axle and impact-tested (i.e., high-strain-rate tested) specimens taken from this core region were similar: SEM micrographs revealed the presence of features (cleavage features and dimples) that are characteristic of mixed-mode (brittle and ductile) fracture.

In spite of evidence supporting the validity of the accident-caused-axle-failure scenario, the plausibility of the other (axle-failure-caused-the-accident) scenario (scenario 2) was also explored. This latter scenario assumes that a fatigue crack or some other slow-crack propagation mechanism initiated the sequence of events that caused the accident. In this case it is important to consider the mechanical characteristics of the portion of the specimen that was last to fail—in this instance, the core region. If failure was due to fatigue, then any increase in loading level of this core region would have occurred relatively slowly, not rapidly as with impact loading conditions. During this gradually increasing load level, fatigue crack propagation would have continued until a critical length was achieved (i.e., until the remaining intact axle cross section was no longer capable of sustaining the applied load); at this time, final failure would have occurred.

On the basis of the tensile test (i.e., slow strain-rate test) performed on this core region, the appearance of the axle fracture surface would be entirely ductile (i.e., dimpled, as per the SEM micrograph of Figure CS3.13). Inasmuch as this core region of the failed shaft exhibited mixed-mode (ductile and brittle) fracture features (both cleavage features and dimples, Figure CS3.5) and not exclusively dimples, the axle-failure-caused-the-accident scenario was rejected.

SUMMARY

This case study was devoted to a failure analysis, which detailed an investigation conducted on a failed rear axle of a light pickup truck that had overturned; the problem was to determine whether the accident resulted from this failure or vice versa. Impact and tensile specimens were fabricated from outer-perimeter and interior regions of the axle, which were subsequently tested. On the basis of scanning electron and metallographic examinations of the actual failed axle surface, as well as the surfaces of these test specimens, it was concluded that the accident caused the axle failure.

REFERENCE

Handbook of Case Histories in Failure Analysis, Vols. 1 and 2, ASM International, Materials Park, OH, 1992.

Case Study 4 Artificial Total Hip Replacement

Learning Objectives

After studying this case study, you should be able to do the following:

1. Name the three components found in most artificial hips, and for each, list its specific materials requirements.
2. For each of these components, name the specific material(s) used and note their requisite characteristic(s)/property (properties).
3. Name and describe the two artificial hip fixation techniques.
4. Name the four artificial hip replacement systems.

CS4.1 ANATOMY OF THE HIP JOINT

As a prelude to discussing the artificial hip, let us first briefly address some of the anatomical features of joints in general and the hip joint in particular. The joint is an important component of the skeletal system. It is located at bone junctions, where loads may be transmitted from bone to bone by muscular action; this is normally accompanied by some relative motion of the component bones. The articulating (or connecting) surface of each joint is coated with cartilage; synovial fluid lubricates and provides an interface with a very low coefficient of friction that facilitates the bone-sliding movement.

The human hip joint (Figure CS4.1) occurs at the junction between the pelvis and the upper leg (thigh) bone, or femur. A relatively large range of rotary motion is permitted at the hip by a ball-and-socket type of joint; the top of the femur terminates in a ball-shaped head that fits into a cup-like cavity (the acetabulum) within the pelvis. An x-ray of a normal hip joint is shown in Figure CS4.2*a*.

Damage and disease to this joint can be painful and disabling and can diminish range of motion. For example, fracture may occur at the narrow region just below the head. Figure CS4.2*b* is an x-ray of a fractured hip; two arrows show the ends of the fracture line through the femoral neck. The hip may also develop osteoarthritis, a

Figure CS4.1 Schematic diagram of human hip joint and adjacent skeletal components.

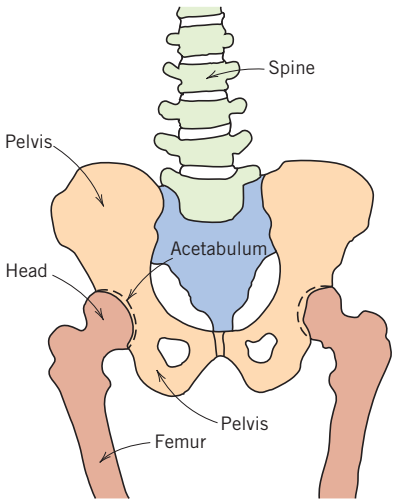

Willsie/iStockphoto

(a)

Willsie/iStockphoto

(b)

Figure CS4.2 X-rays of (*a*) a normal hip joint; (*b*) a fractured hip joint (the two arrows show the ends of one fracture surface); and (*c*) an osteoarthritic hip joint.

ISM/Phototake

(c)

degenerative ailment in which the protective and lubricating cartilage loses some of its resiliency and wears down over time. Eventually bone ends begin to rub against one another (Figure CS4.2*c*), which changes lead to an inflamed and painful joint.

Damaged and diseased hip joints have been replaced with artificial or prosthetic ones, with moderate success, since the late 1950s. *Total hip arthroplasty* (*THA*) [also called *total hip replacement* (*THR*)] surgery involves removing the head, the upper portion of the femur, and some of the bone marrow at the top of the remaining femur

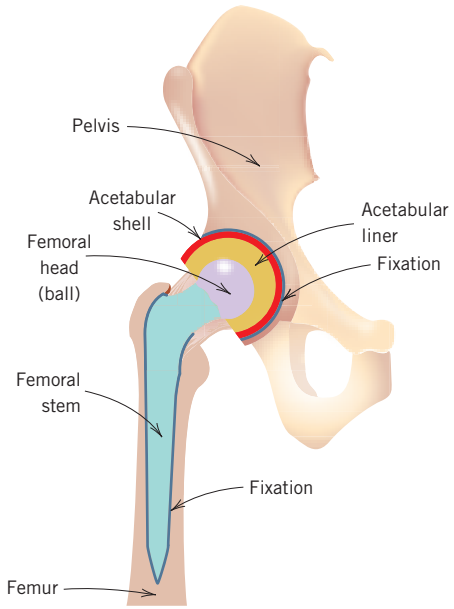

(a)

Courtesy of The Orthopedic Speciality Hospital, Murray, Utah

(b)

Figure CS4.3
(*a*) Schematic diagram and (*b*) x-ray of an artificial total hip replacement.

segment.[12] In addition, the medullary canal of the femur is reamed out in order to accommodate the stem of the prosthesis. Into this hole within the center of the femur a metal anchorage stem is secured that has the ball portion of the joint at its other end; the geometry of this ball-stem component is designed so as to replicate the upper end of the femur. In addition, the replacement cup socket must be attached to the pelvis. This is accomplished by removal of the old cup and its surrounding bone tissue. The new socket is affixed into this recess.[13]

A schematic diagram of the artificial hip joint is presented in Figure CS4.3*a*; Figure CS4.3*b* shows an x-ray of a total hip replacement. In the remainder of this case study we discuss material constraints and those materials that have been used with the greatest degree of success for the various artificial hip components.

CS4.2 MATERIAL REQUIREMENTS

There are three basic components to the artificial hip: (1) a femoral stem, (2) a femoral head (or ball) that attaches to this stem, and (3) an acetabular socket system that is affixed to the pelvis (Figure CS4.4). Some designs call for the stem and ball to be a one-piece unit; however, most often designs are modular and two-piece. In addition, the acetabular socket is frequently a two-unit fixture: a dome-shaped liner (cup or insert) that interfaces

[12]Procedures other than the THA are available to repair hip joints. For example, if a single component of the hip joint is damaged or diseased, a partial hip replacement may be the recommended course of action. The most common of these is for the case wherein the head is replaced and the acetabulum (which is unimpaired) is left intact.

In another procedure, termed "resurfacing," the acetabular socket is replaced (as with THA), whereas the ball is covered (or "resurfaced") with a hemispherical cap made of one of the materials that is normally used for the ball.

[13]Many of today's hip replacement surgeries are computer assisted. From x-rays of the patient's hip anatomy, this technology generates a body map that guides the surgeon in his/her selection of the size and shape of replacement components as well as their positions and orientations. This procedure facilitates the use of a smaller incision and provides higher precision than is possible with the naked eye.

Another recent surgical innovation is the use of a robotic arm to assist the surgeon with bone preparation of the hip joint and placing the implant components in optimal positions and orientations.

with the ball, and a backing shell (or sleeve) that provides for attachment of the liner to the socket cavity (that was carved out of the pelvic bone); the two-piece configuration is represented in the photograph of Figure CS4.4. Each of these components is available in a variety of sizes so as to accommodate different body sizes and types.

The property constraints on materials to be used for these elements are very stringent because of the chemical and mechanical complexity of the hip joint. Some of the requisite material characteristics will now be presented.

Materials selected for these artificial hip components must biocompatible with body tissues—viz., they must be corrosion resistant, and they must not elicit rejection reactions or generate toxic substances.

The bones and replacement components within the hip joint must support forces that originate from outside the body, like those due to gravity; in addition, they must transmit forces that result from muscular action such as walking. These forces are complex and fluctuate with time in magnitude, in direction, and in rate of application. Thus, mechanical characteristics such as modulus of elasticity, yield strength, tensile strength, fatigue strength, fracture toughness, and ductility are all important considerations relative to the materials of choice for the prosthetic hip. For example, the material used for the femoral stem should have minimum yield and tensile strengths of approximately 500 MPa (72,500 psi) and 650 MPa (95,000 psi), respectively, and a minimum ductility of about 8%EL. In addition, the fatigue strength (for bending stresses that are fully reversed)[14] should be at least 400 MPa (60,000 psi) at 10^7 cycles. For the average person, the load on the hip joint fluctuates on the order of 10^6 times per year. In addition, if the modulus of elasticity of the prosthetic material is much greater than that of bone, stress shielding and the resultant deterioration of the surrounding bone tissue may occur; this could lead to implant failure, a second (or revision) surgery, and the implantation of another device.

Furthermore, since the ball-and-cup articulating (or bearing) surfaces rub against one another, wear of these surfaces is minimized by using very hard materials. Excessive and uneven wear can lead to a change in shape of the articulating surfaces and cause the prosthesis to malfunction. In addition, particulate debris will be generated as the articulating

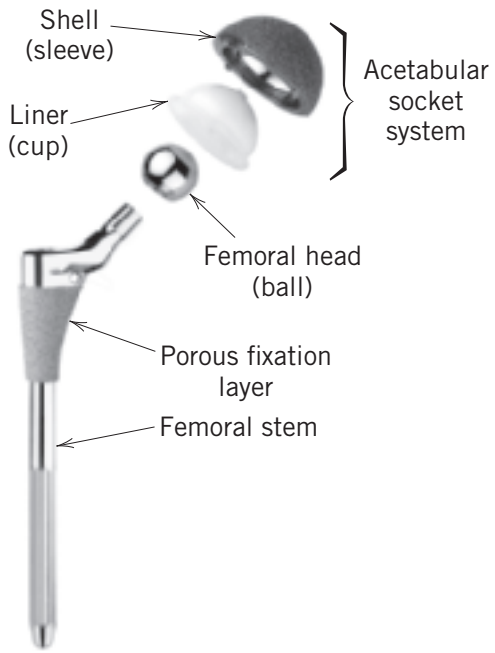

Figure CS4.4 Photograph showing the components of an artificial total hip replacement (in exploded perspective).
(From Davis, J. R., & ASM International, *Handbook of Materials for Medical Devices*. Materials Park, OH, 2003. Figure 3, page 5.)

[14]A schematic stress-versus-time plot for a full-reversed stress cycle is presented in the Cyclic Stresses section (under the Fatigue heading) of the Failure chapter in the print textbook.

surfaces wear against one another; accumulation of this debris in the surrounding tissues can also lead to inflammation.

Frictional forces at these rubbing or bearing faces should also be minimized to prevent loosening of the femoral stem and acetabular cup assembly from their stabilized positions. If these components do become loose over time, the hip joint will experience premature degradation that may require it to be replaced.

Three final important material factors are density, property reproducibility, and cost. It is highly desirable that lightweight components be used, that material properties from prosthesis to prosthesis remain consistent over time, and, of course, that costs of the prosthesis components be reasonable.

Ideally, an artificial hip that has been surgically implanted should function satisfactorily for the life of the recipient and not require replacement. For current designs, lifetimes range between 15 and 25 years. Although this is a substantial improvement from the previous 5- to 10-year figures, longer lifetimes are still desirable.

One final requirement for implant materials is that they be nonmagnetic (i.e., not exhibit ferromagnetic or ferrimagnetic behavior[15]). A frequently used medical diagnostic tool is MRI (magnetic resonance imaging) spectroscopy, a medical test in which the patient is subjected to a very strong magnetic field. The presence of any ferromagnetic/ferrimagnetic materials implanted in the patient will disrupt the applied magnetic field and render MRI spectroscopy unusable. In addition, the magnitudes of these magnetic fields are such that significant forces may be brought to bear on any magnetic implant materials, which may loosen the implant and/or harm the patient. Ferromagnetic materials that should be avoided for implant applications include some ferrous alloys (i.e., ferritic and martensitic stainless steels) and alloys having high contents of nickel and/or cobalt.

CS4.3 MATERIALS EMPLOYED

Femoral Stem

Early prosthetic hip designs called for both the femoral stem and ball to be of the same material—a stainless steel (316LVM). Subsequent improvements have been introduced, including the use of materials other than stainless steel and, in addition, constructing the stem and ball from different materials. Indeed, stainless steel is rarely used in current hip implants.

Today's femoral stems are constructed from titanium and cobalt–chromium–molybdenum alloys. Three wrought titanium alloys are used:

- Ti–6Al–4V ELI (ASTM F136, UNS R56401)
- Ti–12Mo–6Zr–2Fe (ASTM F1813, UNS R58120)
- Ti–6Al–7Nb (ASTM F1295, UNS R56700)

The single wrought cobalt–chromium–molybdenum alloy—Co–28Cr–6Mo—is available in low- and high-carbon contents; their respective designations are ASTM F1537 (alloy 1, UNS R31537) and F1537 (alloy 2, UNS 31538). Although the high-carbon alloy has a greater hardness, the low-carbon one is normally used for stems.

Compositions and mechanical properties of these alloys are contained in Tables CS4.1 and CS4.2.

Furthermore, Ti and Co–Cr–Mo alloy stems are typically fabricated by forging.

Titanium alloys are often preferred for stems. They are extremely biocompatible; there are virtually no reactions with surrounding tissue. In addition, the corrosion resistance of these alloys is excellent. And, as Table CS4.2 notes, their moduli of elasticity are significantly lower than the value for the Co–Cr–Mo alloys. Alloy ASTM 1813 has a modulus of elasticity (74–85 GPa) lower than that of stainless steel, as well as Co–Cr–Mo

[15]The phenomena of ferromagnetism and ferrimagnetism are discussed in the Magnetic Properties chapter of the print textbook.

Table CS4.1 Compositions of Metal Alloys Used for Artificial Total Hip Replacements

Alloy			
Name	*ASTM Designation*	*UNS Designation*	*Composition[a] (wt%)*
		Stainless Steel	
316LVM[b]	F138	S31673	Fe (bal), 0.03 C, 17.00-19.00 Cr, 13.00-15.00 Ni, 2.25-3.00 Mo, 2.0 Mn, 0.50 Cu, 0.10 N, 0.025 P, 0.75 Si, 0.010 S
		Cobalt-Chromium Alloy	
Co-28Cr-6Mo[c]	F1537	R31537	Co (bal), 26.0-30.0 Cr, 5.0-7.0 Mo, 1.0 Ni, 0.75 Fe, 0.14 C, 1.0 Si, 1.0 Mn, 0.25 N
		Titanium Alloys	
Ti-6Al-4V ELI[d]	Fl36	R56401	Ti (bal), 5.5-6.5 Al, 3.5-4.5 V, 0.25 Fe, 0.08 C, 0.13 O, 0.012 H, 0.05 N
Ti-12Mo-6Zr-2Fe (TMZF)	F1813	R58120	Ti (bal), 10.0-13.0 Mo, 5.0-7.0 Zr, 1.5-2.5 Fe, 0.05 C, 0.28 O, 0.020 H, 0.05 N
Ti-6Al-7Nb	F1295	R56700	Ti (bal), 5.50-6.50 Al, 6.50-7.50 Nb, 0.25 Fe, 0.08 C, 0.20 O, 0.009 H, 0.05 N, 0.50 Ta

[a]Single values are maximum values unless indicated otherwise.

[b]In the "LVM" abbreviation, "L" denotes low-carbon content while "VM" indicates that the alloy has been vacuum melted.

[c]Another Co-28Cr-6Mo alloy is also used, which has a higher carbon concentration (0.15-0.35 wt%) and designated as UNS R31538.

[d]"ELI" is the abbreviation for "extra-low "interstitial", which means that the concentrations of interstitial impurities such as C, N, and O are maintained at very low levels. Although the presence of these impurities increases strength (by solid-solution strengthening), ductility may be reduced to unacceptable levels.

Source: Data in this table were extracted from the ASTM International standards referenced, copyright ASTM International, 100 Barr Harbor Drive, West Conshohocken, PA 19428. The complete standards may be obtained from ASTM International, www.astm.org.

Table CS4.2 Mechanical Properties of Metal Alloys That Are Used as Biomaterials

Name	*ASTM Designation*	*Condition*	*Modulus of Elasticity (GPa)*	*Yield Strength (MPa)*	*Tensile Strength (MPa)*	*Ductility (%EL)*
			Stainless Steel			
316LVM	F138	Cold worked	193	690	860	12
			Cobalt-Chromium Alloys			
Co-28Cr-6Mo	F1537	Annealed	240	517	897	20
		Hot worked	240	700	1000	12
		Warm worked	240	827	1172	12
			Titanium Alloys			
Ti-6Al-4V ELI	F136	Annealed	115	760–795	825–860	8–10
Ti-12Mo-6Zr-2Fe (TMZF)	F1813	Soln. annealed	74–85	897	932	12
Ti-6Al-7Nb	F1295	Annealed	110	800	900	10
		Hot worked	110	800	900	10
		Cold worked	110	800	1100	10

Source: Data in this table were extracted from the ASTM International standards referenced, copyright ASTM International, 100 Barr Harbor Drive, West Conshohocken, PA 19428. The complete standards may be obtained from ASTM International, www.astm.org.

Photograph courtesy of Laurie Bray

Figure CS4.5 Photograph showing a metal stem–ceramic ball two-piece hip replacement unit.

and other titanium alloys. Thus, titanium alloy stems are less prone to induce stress shielding and its attendant bone loss. Furthermore, the titanium alloys are more resistant to failure by fatigue.

Femoral Head (Ball)

Because frictional forces are generated at the ball-cup (or bearing) interface, materials chosen for this component must be wear-resistant; any wear products such as submicroscopic particles may cause infection and lead to inflammatory reactions.

Both metals and ceramic materials are used for this femoral ball. Most metal balls are made of the Co–28Cr–6Mo (high-carbon) alloy described earlier. Titanium alloys are not suitable because their wear resistance is poor. The photograph of Figure CS4.4 is shows a metallic ball–metallic stem two-piece device.

Recent prosthetic hip designs call for balls to be made of a highly-polished ceramic material, which is very hard and wear resistant. The ceramic material of choice is a transformation-toughened alumina—alumina to which has been added small particles of yttria-stabilized tetragonal zirconia (Y-TZP).[16] Other oxide additives (SrO and Cr_2O_3) further enhance fracture toughness; these materials form small platelike crystals that deflect advancing cracks. For a ceramic, this material has a relatively high fracture toughness (approximately 6.5 MPa $\sqrt{m}$).[17] Of course this metal stem–ceramic ball component will necessarily be a two-piece unit, as shown in Figure CS4.5.

Acetabular Socket System

Besides biocompatibility, the primary requisite of a material used for the bearing face of the acetabular socket is wear resistance; in addition, a low coefficient of friction is desired so as to minimize frictional forces generated during articulation as the ball rotates within the socket. The material used for this liner or cup may be the same as for the ball as discussed in previous paragraphs—the high-carbon Co–28Cr–6Mo

[16]The mechanics of transformation toughening are discussed in the Ceramic-Matrix section found in the Composites chapter of the print textbook.

[17]The trade name of this zirconia-toughened alumina ceramic is BioLox Delta.

alloy or the zirconia-toughened alumina ceramic. Alternatively, ultra-high-molecular-weight polyethylene has been incorporated into recent designs. The wear and oxidation resistance of this material are excellent as a result of a highly crosslinked structure; crosslinking is induced by radiation. UHMWPE is the cup material for the hip design shown in Figure CS4.4.

No shell is required for Co–Cr–Mo alloy liners—the liner is fastened directly to the pelvis. On the other hand, both ceramic and UHMWPE liners are attached to shells, which, in turn, are affixed to the pelvis. (Shell-to-pelvis fixation techniques are discussed later.) Shells are made of the same titanium alloys used for stems; furthermore, some type of locking mechanism is used to secure the liner to the shell.

CS4.4 FIXATION

One important challenge for total hip replacements is fixation—secure attachment of both the femoral stem to the femur and the acetabular socket assembly to the pelvis. Insufficient fixation of either component ultimately leads to a loosening of that component and the accelerated degradation of the joint. Two types of fixation are used for hip joints: *cemented* and *cementless*.

Cemented Fixation

For cemented fixation, attachment is accomplished using a bone cement—poly(methyl methacrylate)—that is polymerized in situ during surgery. The polymerization reaction must be carefully controlled because the heat generated can lead to bone-tissue damage. Furthermore, the formation of a mechanically sound cement-to-bone bond and a long bond lifetime are, to a large degree, dependent on the surgeon's knowledge of and experience with cements as well as his/her technique—e.g., bone preparation, cement preparation, and cement delivery. A variety of poly(methyl methacrylate) formulations are available that have different viscosities and working and setting characteristics.

The principal advantage afforded by cemented fixation is immediate prosthesis stabilization—the patient is allowed to walk the day after surgery. The usual practice is to use cemented fixation on patients who have relatively low bone densities (e.g., older patients).

Cementless Fixation

For cementless (or biological) fixation, surfaces of the femoral stem and socket shell are coated with a thin textured and highly porous metal layer[18]; after implantation, fixation occurs as new bone tissue grows into and infiltrates this porous network. Cementless prosthesis stabilization takes longer than cemented stabilization because bone ingrowth is a slow process; consequently, it is necessary to restrict a patient's weight-bearing activities for at least several days after surgery. As a general rule, uncemented prostheses are preferred for younger patients who have relatively high bone densities.

For some cementless designs, mechanical stability during bone ingrowth may be accomplished by screwing this assembly directly into the pelvis—screw holes are incorporated into the shell. (Securement screws may be noted in the x-ray of a THR shown in Figure CS4.3*b*.)

Bone ingrowth is influenced by pore size. For pore sizes less than about 50 μm, blood vessel development is restricted and bone ingrowth is not possible. Ingrowth is slow, inconsistent, and of poor quality when pore size exceeds 400 μm.

Coating material and application technique vary from one manufacturer to another. Commercially pure titanium is the most common coating material, although tantalum is also used. The coating may be in the form of metal beads that are sintered onto the

[18]This thin fixation layer is a highly porous implant, which may be observed on the top portions of the femoral stems shown in Figures CS4.4 and CS4.5.

shell surface; coatings are also applied by electron beam melting.[19] Furthermore, some manufacturers use a proprietary arc deposition technique.

The quality of cementless fixation is further improved by applying onto this porous metal surface layer a coating of hydroxyapatite, one component of bone. This treatment serves to accelerate rate of ingrowth as well as improve bond strength (even under loading conditions).

CS4.5 HIP REPLACEMENT SYSTEMS

Prior to a hip replacement, it is the surgeon's responsibility to decide which combination of bearing (head and liner) materials to use. Each surgeon's preference depends on his/her experience, as well as the recipient's age and anatomy. Furthermore, each manufacturer has its own set of models or systems. These fall into the following four categories: metal-on-metal (metal head, metal liner—abbreviated "MoM"), metal-on-polyethylene (metal head, crosslinked UHMWPE liner, "MoP"), ceramic-on-polyethylene ("CoP"), and ceramic-on-ceramic ("CoC"). A schematic representation of these possibilities is shown in Figure CS4.6.

- Metal-on-metal—For most of today's MoM implants, the Co–Cr–Mo alloy is used for both bearing faces. This alloy is very hard and gives rise to wear rates of about 0.01 mm/yr. Wear products from MoM implants pose health concerns. Co and Cr ions are released into the blood and are transported throughout the body; in addition, concentrations build up over time. Currently there are no clinical data to indicate that these metal ions

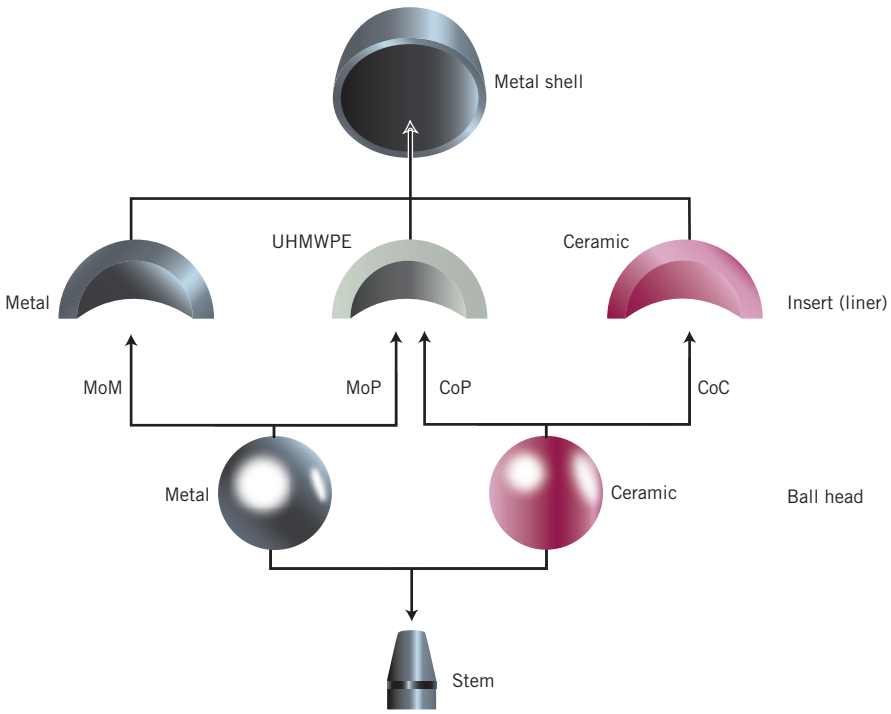

Figure CS4.6 Diagram representing possible hip-replacement systems based on femoral head-acetabular liner material combinations. "MoM" = metal-on-metal, "MoP" = metal-on-polymer, "CoP" = ceramic on polymer, and "CoC" = ceramic-on-ceramic.

[19]For electron beam melting, a thin layer of powder particles of the alloy, melted by an electron beam in a high vacuum, is laid down on the surface of the implant.

lead to increased incidences of cancer or other diseases.[20] Large femoral heads may be used for MoM implants, which reduces the likelihood of dislocation (i.e., when the head becomes dislodged from its socket). And, again, liner shells are not necessary.

- Metal-on-polyethylene—MoP implants are the least expensive and most commonly used. As noted earlier, heads are made of the Co–Cr–Mo alloy. Wear rate for this MoP bearing combination is on the order of 0.1 mm/yr, an order of magnitude greater than for the MoM implants.
- Ceramic-on-polyethylene—The head for CoP implants is transformation-toughened alumina, the hardest bearing material, as discussed earlier.[21] Implant longevity is improved by using a vitamin-E stabilized polyethylene. The wear rate for this CoP system is approximately 0.01 mm/yr.
- Ceramic-on-ceramic—On account of the transformation-toughened ceramic's extreme hardness, wear rate of the CoC bearing couple is the lowest of all implant systems—an almost immeasurable 0.0001 mm/yr. Furthermore, no wear products are generated during articulation, and failure rates are low. Active individuals and relatively young patients are the best candidates for CoC implants.

As a final note: total hip replacements are said to have been the major orthopedic achievement in the 20th century! It is awe-inspiring that THR surgery consistently and, in most cases, completely restores normal functionality to damaged or diseased hips. Before the advent of THR surgery, persons who had serious hip damage or disease were incapacitated for the rest of their lives.

SUMMARY

- Most artificial hip replacement designs call for three components: femoral stem, femoral head (ball), and an acetabular cup–liner-backing shell assembly.
  - Most of today's femoral stems are constructed from titanium alloys; in some cases Co–Cr–Mo alloys are used.
  - Materials for the ball component are made of zirconia-toughened alumina as well as Co–Cr–Mo alloys.
  - Acetabular liners are made of highly crosslinked UHMWPE as well as zirconia-toughened alumina and Co–Cr–Mo alloys.
- Fixation of the stem and acetabular cup may be cemented or cementless.
  - Cemented fixation uses bone cement [poly(methyl methacrylate)] that is polymerized in situ during the surgery.
  - For cementless, surfaces of the femoral stem and socket shell are coated with a thin and highly porous metal layer into which bone tissue grows.

REFERENCES

Davis, J. R. (Editor), *Handbook of Materials for Medical Devices*, ASM International, Materials Park, OH, 2003.

Park, J., and R. S. Lakes, *Biomaterials: An Introduction,* 3rd edition, Springer, New York, NY, 2007. Chapter 14.

Ratner, B. D., A. S. Hoffman, F. J. Schoen, and J. E. Lemons (Editors), *Biomaterials Science: An Introduction to Materials in Medicine*, 3rd edition, Elsevier Academic Press, San Diego, CA, 2013. Section II-5.6.

[20]Recalls of Co–Cr–Mo metal-on-metal hips were recently issued, in response to class-action lawsuits filed against manufacturers of this type of hip replacement. Chromium and cobalt levels in the blood of implant recipients have been found to be unusually high, which may have resulted from abrasive wear and the generation of metal debris. Many recipients experienced some of the following symptoms: pain, disturbed sleep, mood swings, anxiety, hearing loss, and/or visual problems.

[21]Some of the first-generation implanted ceramic femoral heads failed (fractured), which necessitated immediate revision (i.e., surgery and replacement). Consequently, a recall was issued with the temporary cessation of ceramic head implantation. Investigations revealed that the failures resulted from structural defects introduced during fabrication. This problem was corrected, and the recall lifted.

Case Study 5 Intraocular Lens Implants

Learning Objectives

After studying this case study, you should be able to do the following:

1. In addition to biocompatibility, cite three properties required of materials that are used for intraocular lenses.
2. Name five different material types (including copolymers) that are used for intraocular lenses. Note distinctive characteristics of each.

CS5.1 ANATOMY OF THE EYE

We begin this case study by discussing the anatomical components of the human eye some of which are shown in the schematic diagram of Figure CS5.1. Light enters the eye through the cornea—the transparent outermost layer. From here it passes into the anterior chamber (which is filled with aqueous humor) and then through the pupil, the opening located in the center of the iris. The iris is a thin, circular aperture, which acts as a shutter—that is, by opening and closing (i.e., changing diameter) it regulates the amount of light that reaches the pupil.[22] Next is the posterior chamber—the narrow space located between the iris and the lens. The lens, which resides in a chamber refracts the light beam so that it focuses (or converges) on the retina, the light-sensitive lining that covers the inner rear surface of the eye (Figure CS5.2).[23] Attached to the periphery of the lens are ciliary muscles; lens shape and thickness change as these muscles contract and relax. This action changes the focal length of the lens, which allows the eye to focus on objects that are positioned at a variety of distances. The degree to which the eye is able to make these focusing adjustments is called *accommodation*. As one ages, flexibility of the lens decreases, as does the accommodation of the eye—it becomes more difficult to focus on nearby objects.

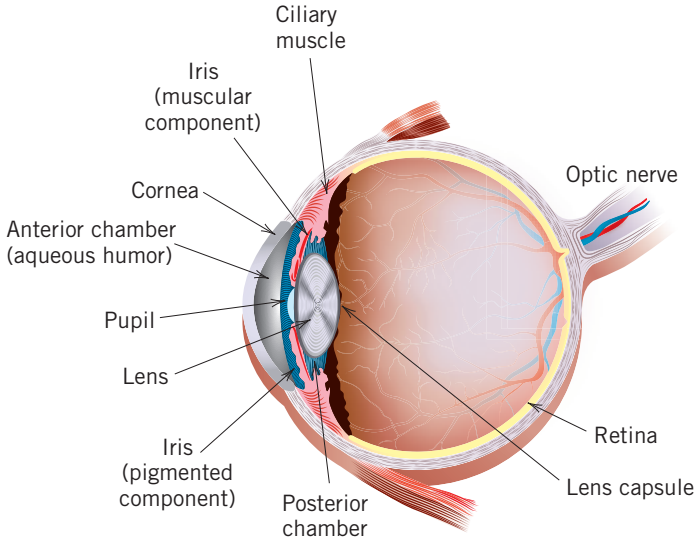

Figure CS5.1 Schematic diagram of the human eye; labels are affixed to components discussed in this case study.

[22]One's eye color is the same as the color of the iris.

[23]Some refraction also occurs at the cornea.

Figure CS5.2 Schematic diagram showing the focusing a beam of light onto the retina.

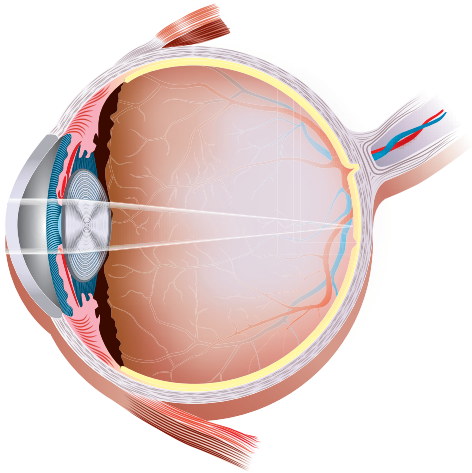

CS5.2 CATARACTS AND CATARACT SURGERY

One of the common eye diseases (especially for older people) is the formation of cataracts, wherein the natural lens of the eye becomes clouded and increasingly opaque with the result that vision is impaired—the clouded lens scatters an incoming light beam such that it fails to focus on the retina (Figure CS5.3). If cataracts are left untreated blindness will result.[24] Figures CS5.4*a* and CS5.4*b*, respectively, are photographs of a normal eye and an eye that has a cataract in an advanced stage of development. Glasses or contact lenses are not capable of restoring vision when a cataract is present—the natural lens must be removed surgically and replaced by an artificial *intraocular lens* (IOL). This "corrective lens" provides the focusing power for normal vision.

The surgical procedure is administered under local anesthesia, and, when performed by an experienced ophthalmologist, takes less than an hour. A small incision (as short as 2 to 3 mm) is made at the edge of the cornea that penetrates into the lens capsule. Through this incision is inserted a small ultrasonic probe that, by vibrating at a high frequency (40,000 Hz), fragments the soft lens tissues (including the cataract) within the lens capsule into small pieces, in a process called phacoemulsification. After phacoemulsification, another small irrigation-aspiration probe is inserted, which dissolves and completely aspirates (sucks out) all of the small tissue fragments from within the lens capsule, which is left intact. At this time the soft (and folded) intraocular

Figure CS5.3 Schematic diagram showing the dispersion of a light beam by a cataract.

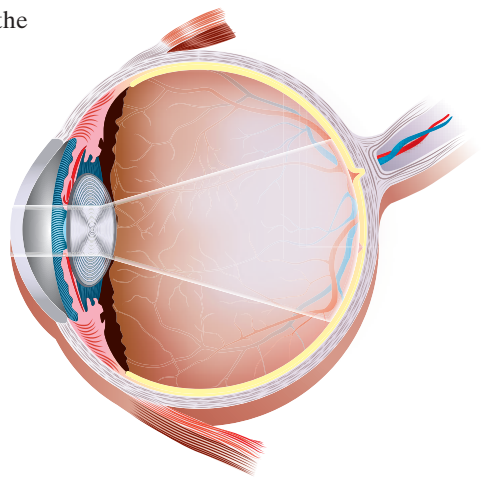

[24]The clouded lens is a cataract.

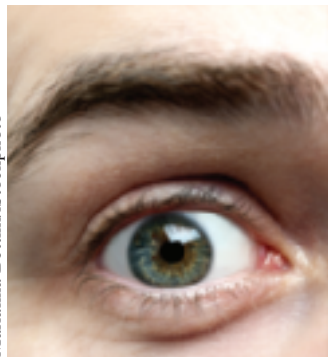

Marianna Bettini/iStockphoto

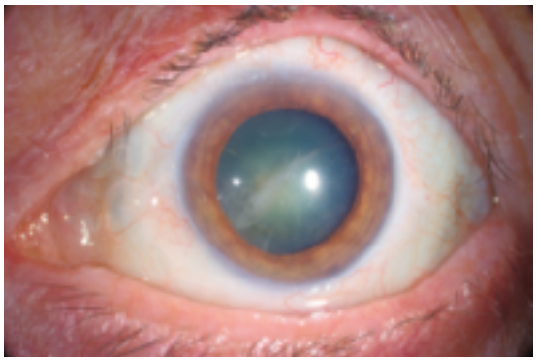

ISM/Phototake

(a) (b)

Figure CS5.4 Photographs of (*a*) a normal eye, and (*b*) an eye with a cataract in an advanced stage of development.

lens is inserted into the lens capsule, correctly positioned, and then unfolded at or near the position of the natural lens using an injector tool. Thus, the IOL implant becomes a permanent part of the eye. It is not necessary to apply sutures to the incision because of its small size.[25]

After implantation, intraocular lenses are designed to restore normal vision including peripheral vision, depth perception, and image size; in many instances it is not necessary for the patient to use corrective lenses (eyeglasses). Figure CS5.5 is a schematic diagram that shows an implanted intraocular lens.

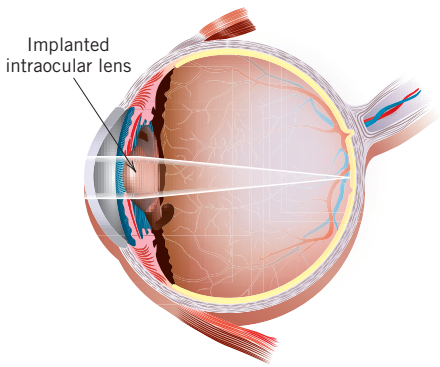

Figure CS5.5 Schematic diagram that shows an implanted intraocular lens and its focusing of a light beam onto the retina.

[25]Several computer-controlled and automated laser cataract surgery systems have recently been developed. Each of these allows the surgeon to make very precise incisions and also automates lens removal and IOL insertion procedures. High-resolution cross-section profiles of the anterior region of the eye are first created and stored using a video imaging technique. These images are used to guide the laser (termed a "femtosecond laser") to make an incision into the lens capsule; incision location, length, and depth are precisely determined. The laser is then used to fragment the lens into a predetermined pattern; this permits efficient phacoemulsification and removal through this incision. Corneal incisions having predetermined dimensions and geometries are also created with the laser; these are used for insertion and placement of the IOL and, in addition, are self-healing.

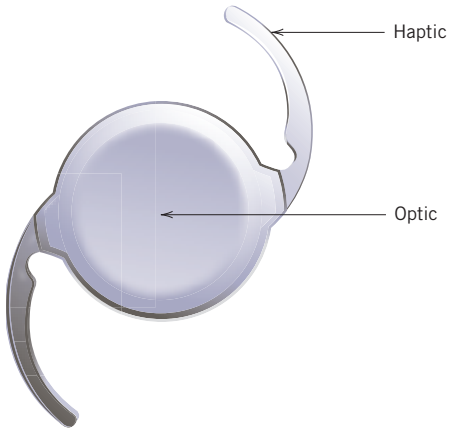

Figure CS5.6 Diagram of a typical intraocular lens; haptic and optic components are noted.

CS5.3 IOL COMPONENTS, TYPES, AND FEATURES

Most intraocular lenses consist of a circular focusing lens to which is attached, on opposite sides, two plastic protrusions, called *haptics* (Figure CS5.6). After implantation and unfolding of lens assembly, these haptics hold the lens in position and prevent it from rotating within the capsular bag. Haptics may be an integral part of the IOL (as a one-piece unit), or separate members (for a three-piece unit). Furthermore, for three-piece lenses, the haptics and an optic portion may be made of different materials. Several intraocular lens designs are shown in Figure CS5.7. Figure CS5.8 is a photograph of an implanted IOL.

With regard to optical function, five types of intraocular lenses are currently available: *monofocal*, *multifocal, accommodating*, *toric*, and *aspheric*. Table CS5.1 lists some currently available IOLs—their types, product names, and biomaterial(s) used, and in some cases important features.

- Monofocal IOLs have relatively narrow depths of focus—that is, they correct vision for one distance only—near, intermediate, or far. The patient needs to wear glasses for correction of other distances.
- Multifocal intraocular lenses correct vision simultaneously for multiple distances (i.e., have a high degree of accommodation), and may eliminate the need for eyeglasses.

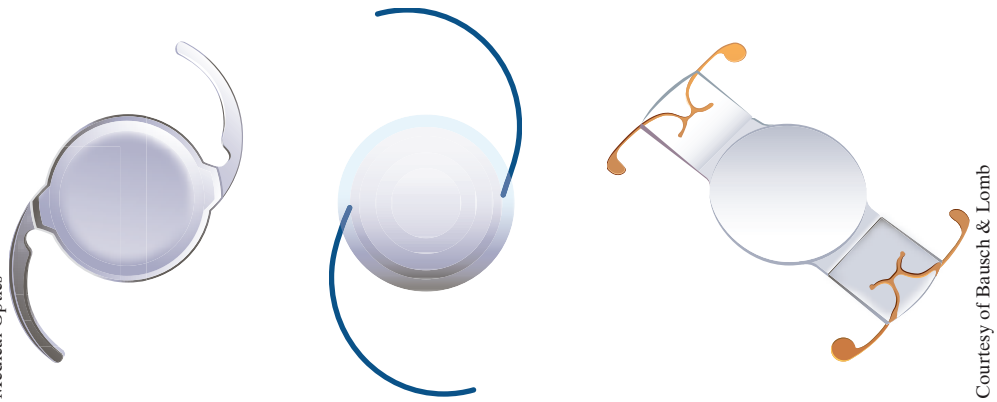

Figure CS5.7 Photographs/schematic diagrams of three intraocular lens designs: (*a*) single-piece toric, (*b*) three-piece multifocal, and (*c*) Crystalens accommodating.

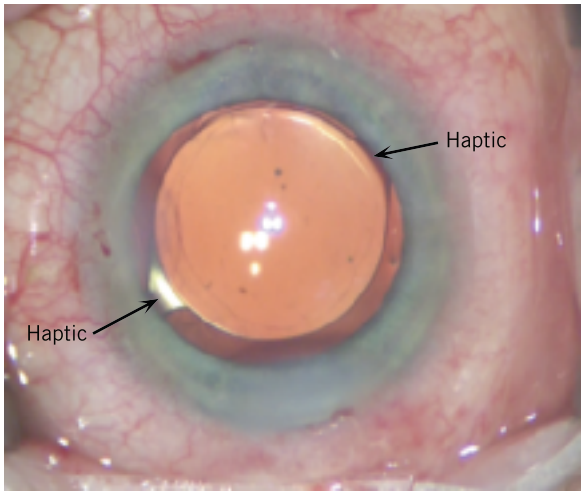

Courtesy of Dr. R. J. Cionni, The Eye Institute of Utah

Figure CS5.8 Photograph of an implanted intraocular lens.

- Unlike other lens types, accommodating IOLs focus in the same manner as the natural lens—they are attached to the ciliary muscles, which when flexed, move the lens forward and backward within the capsule. This type of lens corrects for distance and midrange near vision, but not for close vision as do the multifocal lenses. At this time, only Bausch & Lomb's Crystalens IOL (Table CS5.1) has been approved by the FDA; however, other accommodating lenses have been developed and are available outside the U.S.
- Toric lenses are contoured so as to correct for any astigmatism.[26] Because correction power varies from region to region of the lens, it is imperative that the lens be positioned in a very precise and specific orientation in the lens capsule. Distance vision is also corrected with these lenses; however near vision is not, and, therefore, glasses are needed for close-vision correction.
- Aspheric IOLs compensate for any spherical aberration of the cornea.[27] As the name suggests, surface profiles of these IOLs are not spherical (i.e., they are aspherical); rather, their profiles are contoured so as to counteract the cornea's spherical aberrations. These lenses also improve contrast sensitivity.

Inasmuch as no lens is able to adequately correct for all distance ranges as well as astigmatism and visual aberrations, a different lens type may be implanted in each eye of the patient in order to provide a better mix of corrective features than is possible with a single lens. One example is the implantation of a multifocal IOL in one eye and an accommodating IOL in the other. Near (e.g., reading) vision is optimized by the multifocal lens, whereas the accommodating one corrects for midrange and distance vision.

Undesirable effects that patients may experience from their IOL implants include glare and halos around lights, and also night vision problems. These problems are minimized for some IOL designs.

---

[26]Astigmatism is an optical condition that produces blurred vision—in our case light rays refracted by the cornea do not meet at a single point. Astigmatism results from an irregularity in the cornea—the shape of the cornea has a cylindrical component rather than being completely spherical (as with the normal eye).

[27]Spherical aberration is an optical phenomenon wherein a region of an image is out of focus because not all rays of light focus at the same point. Those rays passing through the outer periphery of the lens focus at a point nearer to the lens than those rays passing through the lens center.

Table CS5.1 Names, Types, and Characteristics of Intraocular Lenses

Manufacturer	*Product Name*	*Type of IOL*	*Biomaterial/Features*
Bausch & Lomb	Crystalens	Multifocal (single-focus accommodating)	Biosil (solid silicone)
Alcon	AcrySof IQ Monofocal	Monofocal	Phenylethyl acrylate–phenylethyl methacrylate crosslinked copolymer
	AcrySof IQ ReSTORE	Multifocal	Acrylate–methacrylate copolymer, apodized (tapered diffractive steps)
	AcrySof IQ Aspheric	Aspheric	Hydrophobic acrylate–methacrylate copolymer
	AcrySof IQ Toric	Monofocal, toric, aspheric	Hydrophobic acrylate–methacrylate copolymer
Abbott Medical Optics	ReZoom	Multifocal	High-index acrylic, PMMA haptics, multifocality achieved by a series of rings
	Tecnis Multifocal 1-Piece	Multifocal, aspheric	Hydrophobic acrylic, multifocality achieved by a series of rings
	Tecnis Multifocal 3-Piece	Multifocal, aspheric	Hydrophobic acrylic, PMMA haptics, multifocality achieved by a series of rings
	Tecnis Acrylic	Aspheric	Hydrophobic acrylic, PMMA haptics
	Tecnis CL Silicone	Aspheric	SLM-2 Silicone, PMMA haptics
Staar Surgical	NanoFLEX Collamer	Aspheric	Collagen/poly-HEMA copolymer; single-piece
	Afinity Collamer	Aspheric	Collagen/poly-HEMA copolymer; three-piece
	Elastimide	Aspheric	Silicone, aspheric, 3-piece, polyimide haptics
	Elastic	Aspheric	Silicone, single-piece
	Toric	Toric	Silicone, single-piece

Source: Manufacturers' data sheets.

CS5.4 MATERIALS EMPLOYED

Materials used for IOLs not only must be biocompatible with eye tissues (and also transparent), but also must have an appropriate refractive index so as to provide adequate focusing power. The ability to absorb ultraviolet (UV) radiation, which can damage eye tissues, is also desirable. This radiation protection is incorporated into virtually all of the IOLs that are currently available. In addition, in order to be compatible with the surgical procedure described previously, materials used for today's IOL materials must be soft and flexible. Also, after insertion into the lens capsule, unfolding of the optic and haptics should be controlled and relatively slow.

Poly(methyl methacrylate) (PMMA) in a rigid form was the mainstay material for many years.[28] However, most of the acrylics in current use for IOLs have a

[28]The discovery that PMMA is biocompatible with eye tissues was accidental. In 1949, an optometrist in London examined some British Royal Air Force pilots who had implanted in their eyes fragments of PMMA from aircraft canopies. He observed that their eyes tolerated the presence of these fragments for several years without any noticeable inflammation or unacceptable biological reactions.

much higher degree of flexibility. For example, one of the early materials of this type is Alcon's AcrySof (or soft acrylic), a proprietary polyacrylic copolymer. Furthermore, haptics for some of the IOLs listed in Table CS5.1 are made of monofilament PMMA.

Over time, calcium deposits form on surfaces of some acrylic IOLs, which leads to opacification—a reduction in the degree of light transmittance through the lens. This opacification problem appeared to be more prevalent in hydrophilic acrylic lenses [those whose surfaces had a high affinity for (or attraction for) water] than for hydrophobic acrylics, which surfaces repelled water molecules.[29] For this reason, a number of the acrylic materials in Table CS5.1 are hydrophobic in character. However, the latest hydrophilic acrylics appear to have overcome this opacification problem, and, in addition, have some advantages over the hydrophobics, including better biocompatibility and optical clarity, resistance to damage during implantation, and protection from biocontamination. This hydrophilic acrylic is poly(2-hydroxyethyl methacrylate) (pHEMA), a hydrogel with a 26% water content. Copolymers composed of the hydrophilic pHEMA and hydrophobic methyl acrylate (having water contents of about 25%) have also been formulated that have higher refractive indexes (and thinner lens designs) and are more mechanically robust and foldable than the pHEMA homopolymer.

The Crystalens accommodating IOL's configuration (Figure CS5.5*c*) is different from that of the other IOLs—at each optic-haptic junction is a hinge, whereas loops are attached to the haptic extremities. Hinges allow for the eye's ciliary muscles to translate the optic forward and backward as the lens focuses on near and far objects. Loops secure and stabilize the IOL within the lens capsule. Both optic and lens components are manufactured of the same material—a proprietary and specially formulated solid silicone called Biosil.

The material used for Staar Surgical's aspheric NanoFLEX and Afinity IOLs is a collagen-pHEMA copolymer (or Collamer). This material is a hydrogel (containing approximately 40% water) that is highly biocompatible. Furthermore, because Collamer's light transmittance characteristics are similar to those of the human eye, there is less likelihood of the occurrence of glare, halos, and poor night vision

Four of the IOLs in Table CS5.1 are made of silicone materials: Abbott Medical Optics' Tecnis CL Silicone, and Staar Surgical's Elastimide, Elastic Lens, and Toric Silicone. These materials have been formulated to meet performance standards required for IOL implants. In addition to biocompatibility, these silicones must have appropriate refractive indices, mechanical properties (e.g., softness and bendability), and UV transmission characteristics.

SUMMARY

- Intraocular lenses are used to restore normal vision after cataract surgery.
- IOLs may improve accommodation and correct visual defects (astigmatism and spherical aberration).
- In addition to being biocompatible and transparent, IOLs must provide adequate focusing power, absorb UV radiation, and be soft and flexible.

[29]Whether an acrylic material is hydrophobic or hydrophilic depends on its chemistry.

- Materials used for IOLs include the following:
  Flexible poly(methyl methacrylate) (PMMA)
  Poly(2-hydroxyethyl methacrylate) (pHEMA) (as a hydrogel)
  pHEMA-methyl methacrylate copolymer
  Collagen-pHEMA copolymer (Collamer)
  Silicone

REFERENCE

Ratner, B. D., A. S. Hoffman, F. J. Schoen, and J. E. Lemons (Editors), *Biomaterials Science: An Introduction to Materials in Medicine*, 3rd edition, Elsevier Academic Press, San Diego, CA, 2013. Section II-5.9B.

Case Study 6 Chemical Protective Clothing

Learning Objectives

After studying this case study, you should be able to do the following:

1. Name and briefly define the two factors that are important to consider relative to the suitability of a material for use for chemical protective clothing.
2. For a chemical protective clothing material, discuss how breakthrough time is related to the diffusion coefficient and material thickness.

CS6.1 INTRODUCTION

A number of commercially important chemicals, when exposed to the human body, can produce undesirable reactions; these reactions may range from mild skin irritation to organ damage or, in the extreme case, death. Anyone who risks exposure to these chemicals should wear chemical protective clothing (CPC) to prevent direct skin contact and contamination. Protective clothing includes at least gloves, but in some instances boots, suits, and/or respirators may be required. This case study involves the assessment of chemical protective glove materials for exposure to methylene chloride.

The choice of a suitable glove material should include consideration of several important factors. The first of these is *breakthrough time*—that is, the length of time until first detection of the toxic chemical species inside the glove. Another key factor is the *exposure rate*—that is, how much of the toxic chemical passes through the glove per unit time. Consideration of both breakthrough time and exposure rate is important. Other relevant material factors include material degradability, flexibility, and puncture resistance. Trade-offs of these several characteristics may be necessary. For example, a thick glove may have a longer breakthrough time and lower exposure rate but be less flexible than a thin glove.

Common commercially available glove materials include natural rubber, nitrile rubber, poly(vinyl chloride), neoprene rubber, and poly(vinyl alcohol) (PVA). Some gloves are *multilayered*, that is, composed of layers of two different materials that take advantage of the desirable features of each. For example, PVA is highly impermeable to many organic solvents but is soluble in water; any exposure to water can soften (and ultimately dissolve) the glove. To counteract this liability, CPC materials have been developed that consist of a thin layer of PVA sandwiched between two layers of a nonpolar polymer such as polyethylene. The PVA layer impedes the diffusion of nonpolar materials (i.e., many of the organic solvents), whereas the polyethylene layers shield the PVA from water and inhibit the permeation of polar solvents (i.e., water and alcohols).

CS6.2 ASSESSMENT OF CPC GLOVE MATERIALS TO PROTECT AGAINST EXPOSURE TO METHYLENE CHLORIDE

Let us consider the selection of a glove material for use with methylene chloride (CH_2Cl_2), a common ingredient in paint removers. Methylene chloride is a skin irritant and may be absorbed into the body through skin; studies suggest that its presence in the body may cause cancer as well as birth defects. Computations are possible of breakthrough time and exposure rate for methylene chloride that is in contact with potential glove materials. In light of the hazardous nature of CH_2Cl_2, any assumptions we make for these calculations are conservative and overestimate the inherent dangers.

Computation of breakthrough time for passage of a hazardous chemical through a chemical protective glove material

The breakthrough time t_b is related to the diffusion coefficient of methylene chloride in the glove material (D) and the glove thickness (ℓ) according to the following equation:

$$t_b = \frac{\ell^2}{6D} \tag{CS6.1}$$

Values of D, ℓ, and t_b (computed using the preceding expression) for several commercially available CPC glove materials are provided in Table CS6.1. Breakthrough times can also be measured directly using appropriate equipment; these measured values are in good agreement with the calculated ones presented in the table.

For exposure-rate computations, we assume that a condition of steady-state diffusion has been achieved, and also that the concentration profile is linear. In fact, at the outset of exposure to methylene chloride, its diffusion through the glove is nonsteady-state, and the accompanying diffusion rates are lower than those calculated for conditions of steady state. For steady-state diffusion, the diffusion flux J is calculated according to Fick's first law as[30]

$$J = -D\frac{dC}{dx} \tag{CS6.2}$$

For a linear concentration profile, this equation takes the form

$$J = -D\frac{C_A - C_B}{x_A - x_B} \tag{CS6.3}$$

We arbitrarily take the A and B subscripts to denote glove surfaces in contact with the methylene chloride and with the hand, respectively. In addition, the glove thickness is $\ell = x_B - x_A$, such that the preceding equation now takes the form

$$J = D\frac{C_A - C_B}{\ell} \tag{CS6.4}$$

Now, the exposure rate r_e is equal to the product of the diffusion flux and total glove surface area (A)—that is,

$$r_e = JA = \frac{DA}{\ell}(C_A - C_B) \tag{CS6.5}$$

Table CS6.1 Characteristics and Costs for Commercially Available Chemical Protective Glove Materials That Are Candidates for Use with Methylene Chloride

Material	*Diffusion Coefficient, D (10^{-8} cm²/s)*	*Glove Thickness, ℓ (cm)*	*Breakthrough Time, t_b (h)*	*Surface Concentration, S_A (g/cm³)*	*Exposure Rate, r_e (g/h)*	*Cost (US$/Pair)*
Multilayer[a]	0.0095	0.007	24	11.1	0.43	4.19
Poly(vinyl alcohol)	4.46	0.075	5.8	0.68	1.15	24.00
Viton rubber	3.0	0.025	0.97	0.10	0.35	72.00
Butyl rubber	110	0.090	0.34	0.44	15.5	58.00
Neoprene rubber	92	0.075	0.28	3.53	125	3.35
Poly(vinyl chloride)	176	0.070	0.13	1.59	115	3.21
Nitrile rubber	157	0.040	0.05	2.68	303	1.56

[a]The trade name for this material is "Silver Shield".

Sources: Manufacturers' data sheets.

[30]See the Fick's First Law section in the Diffusion chapter of the print textbook.

An average-size pair of gloves has an inside surface area of about 800 cm^2. Furthermore, the surface concentration of methylene chloride (i.e., C_A) is equal to its solubility in that polymer (which we denote as S_A); solubility values for several glove materials are also included in Table CS6.1. Now, if we assume that all methylene chloride, upon contact, is immediately absorbed by the skin and swept away by the bloodstream, then C_B takes on a value of 0 g/cm^3.[31] Thus, upon making the preceding substitutions for C_A and C_B into Equation CS6.5, we obtain the following expression for r_e:

Computation of exposure rate of a hazardous chemical that is diffusing through a chemical protective glove material

$$r_e = \frac{DAS_A}{\ell} \tag{CS6.6}$$

Table CS6.1 also includes for these glove materials values of r_e that were determined using Equation CS6.6.

At this point, a key question is: What is an acceptable and safe exposure rate? Based on airborne exposure limits set by the Occupational Safety and Health Administration (OSHA) of the United States, the maximum allowable r_e to methylene chloride is approximately 1 g/h.

Now let us examine and compare computed breakthrough times and exposure rates for the glove materials, as listed in Table CS6.1. First of all, with regard to exposure rate, two of the seven materials meet or exceed the standard set by OSHA (viz., 1 g/h)—multilayer (Silver Shield) and Viton rubber (with r_e values of 0.43 and 0.35 g/h, respectively). Relative to breakthrough time, the multilayer material has the longer t_b (24 h versus about 1 h for the Viton rubber). Furthermore, the multilayer gloves are considerably less expensive (at US$4.19 per pair compared to US$72.00 for Viton rubber, Table CS6.1).

Therefore, of these two glove materials, other relevant characteristics/properties being equal, the one of choice for this application is multilayer Silver Shield. It has a significantly longer breakthrough time and is much less costly than the Viton rubber material, whereas there is very little difference between their exposure rates.

The photograph in Figure CS6.1 shows a pair of Silver Shield gloves.

Figure CS6.1 Photograph of Silver Shield multilayer chemical protective gloves. (Photograph courtesy of North Safety Products, Anjou, Quebec, Canada.)

[31] In most practical situations, $C_B > 0$ g/cm^3 because not all of the methylene chloride that passes through the glove will immediately be absorbed into the skin and removed from the hand by the bloodstream. Thus, the values of r_e we calculate will be greater than the actual exposure rates that the hands experience.

The calculated breakthrough time values presented in Table CS6.1 assumed that the glove material had no previous exposure to methylene chloride. For a second application, some of the methylene chloride that dissolved in the glove during the first exposure probably remains; thus, the breakthrough time will be much shorter than predicted for an unused glove. For this reason, CPC gloves are often discarded after one use.

Always consult an industrial hygiene specialist when selecting chemical protection clothing. These specialists are experts as to what materials are suitable for exposure to specific toxic chemical substances and also with regard to other factors such as material degradability, flexibility, grip, and puncture resistance.

SUMMARY

This case study was concerned with materials to be used for chemical protective clothing—specifically, glove materials to protect against exposure to methylene chloride, a common ingredient in paint removers. Important parameters relative to the suitability of a chemical protective material are breakthrough time and exposure rate. Equations were provided that allow computation of these parameters, and values were determined for seven common protective glove materials. Only two materials {multilayered [poly(vinyl alcohol)/polyethylene] and Viton rubber} were deemed satisfactory for this application.

REFERENCES

Anna, D. H., *Chemical Protective Clothing*, 2nd edition. American Industrial Hygiene Association, Fairfax, VA, 2003.

Forsberg, K., and L. H. Keith, *Chemical Protective Clothing Performance Index,* Wiley, New York, NY, 1999.

Forsberg, K., and S. Z. Mansdorf, *Quick Selection Guide to Chemical Protective Clothing,* 5th edition, Wiley, Hoboken, NJ, 2007.

DESIGN PROBLEM

CS6.D1 Toluene (C_7H_8) is frequently used as a solvent or thinner for oil-based paints. Assess potential CPC glove materials to protect against exposure to toluene. Based on airborne exposure limits set by OSHA, the maximum allowable exposure rate to toluene is approximately 8 g/h. The diffusion coefficients and surface concentrations for toluene in several materials are as follows:

Material	*Diffusion Coefficient, D* (10^{-8} cm^2/s)	*Surface Concentration,* S_A (g/cm^3)
Butyl rubber	61	2.55
Multilayer (Silver Shield)	0.0089	7.87
Neoprene rubber	64	3.53
Nitrile rubber	15	2.68
Poly(vinyl alcohol)	1.28	0.68
Poly(vinyl chloride)	100	0.25
Viton rubber	0.73	2.61

(a) Determine the breakthrough time and exposure rate for each of these materials.

(b) Discuss which of these materials would be appropriate for use as a CPC glove material for toluene.

Index

G

H

I

L

M

N

O

P